LAWRENCE
LIVERMORE
NATIONAL
LABORATORY

LLNL-JRNL-650042

A Comparative Analysis of the Cryo-compression and Cryo-adsorption Hydrogen Storage Methods

G. Petitpas, P. Benard, L. E. Klebanoff, J. Xiao, S. M. Aceves

February 18, 2014

International Journal of Hydrogen Energy

Disclaimer

A Comparative Analysis of the Cryo-compression and Cryo-adsorption Hydrogen Storage Methods

G. Petitpas[1]*, P. Bénard[2], L.E. Klebanoff[3], J. Xiao[2] and S. Aceves[1]

[1]Lawrence Livermore National Laboratory, 7000 East Avenue, Livermore CA 94550, USA

[2]Institut de recherche sur l'hydrogène, Université du Québec à Trois-Rivières, Québec, Canada G9A 5H7

[3]Sandia National Laboratories, 7011 East Avenue, Livermore CA 94550, USA

*Author to whom correspondence should be addressed: petitpas1@llnl.gov; +001 925 423 0348

Abstract:

While conventional low-pressure LH_2 dewars have existed for decades, advanced methods of cryogenic hydrogen storage have recently been developed. These advanced methods are cryo-compressed and cryo-adsorption hydrogen storage that operate in the temperature range 30 – 100K. We present a comparative analysis of the cryo-compressed and cryo-adsorption approaches to hydrogen storage, examining their respective storage densities and dormancies as a function of temperature, pressure and type of cryo-adsorption material. We start by reviewing some basic aspects of LH_2 properties and conventional means of storing it. From there we describe the cryo-compressed and cryo-adsorption hydrogen storage methods, and then explore the relationship between them, clarifying the materials science and physics of the two approaches in trying to solve the same hydrogen storage task and determining the regimes of temperature and pressure when the two methods are at their best.

I. Introduction

Keller et al. [1] have recently provided a compelling argument that if we are going to solve our fuel resource insecurity, political energy insecurity and environmental sustainability problems that accompany our current fossil-fuel-based energy infrastructure, we as a civilization are going to need to turn to hydrogen. In particular, environmental sustainability will only be achieved through a zero-carbon energy solution that hydrogen technology can ultimately provide. We define a zero-carbon energy solution as an energy system in which there is no net release of CO_2 or other greenhouse gases (GHGs) into the atmosphere, either at the point of technical use, or along the path used to produce hydrogen. Unless we have a zero-carbon solution, none of the benefits accrued to a new infrastructure (such as reduction in GHG emissions) can survive growth in either population, or growth in the intensity with which technology uses energy [1]. So, the need is clear for hydrogen-based power technology, and it needs to be a zero-carbon hydrogen technology. The time-scales for technological change and the ~ 50 year horizon associated with our limited fossil fuel resources indicate that we have to start the conversion to a zero-carbon technology like hydrogen now, and we need to be going much faster than we are [1].

As recently reviewed by Klebanoff et al. [2], high efficiency hydrogen energy conversion devices that convert hydrogen into electrical or shaft power are powerful drivers for hydrogen technology. These conversion devices include hydrogen internal combustion engines (ICEs), both spark ignition and turbine hydrogen engines, along with hydrogen fuel cells. Proton exchange membrane (PEM) fuel cells in particular are already finding use in the first fuel cell vehicles, and also commercial use in portable power, backup power, material handling equipment and fuel cell mobile lighting [2]. Hydrogen ICEs have already been demonstrated in light-duty vehicles, with even small production runs made for the BMW Hydrogen 7 vehicle [3].

Different options exist for hydrogen storage and delivery [4]. For chemical manufacturing and laboratory uses of hydrogen, the hydrogen is conveniently stored as room temperature compressed hydrogen gas in appropriately sized cylinders (fabricated from steel, aluminum or composite) at pressures up to ~200 –700 bar. The first hydrogen-powered ground vehicles have typically used compressed gas for on-board storage [5]. These high-pressure tanks are safe and reliable means of storing hydrogen at the pressures for which they were designed. The composite tank manufacturers in particular deserve a lot of credit for producing a high-quality product. For spacecraft applications (i.e. as a rocket propellant) requiring very large quantities of hydrogen, hydrogen is stored in cryogenic LH_2 containment vessels (LH_2 dewars) in large stationary storage facilities and also as part of the launch vehicle itself [6]. No large scale hydrogen distribution infrastructure exists to date, and it may very well be that a large-scale LH_2 infrastructure does arise. Although it typically requires about 30% of the hydrogen fuel energy to liquefy it [7], it might be worth it (in cost and energy) because once liquefied, LH_2 can be transported and dispensed very easily without the need for (currently) expensive pressure vessels, and dispensing hardware rated for high pressure [4]. The overall cost reductions for

transporting LH_2 might make it the physical state of choice for a hydrogen energy infrastructure [8]. The advantages of LH_2 distribution are illustrated in a recent California Air Resources Board (CARB) report [9]. This report predicts future deployment of H_2 fueling stations for different sources of H_2 (liquid delivery, gaseous delivery, or on-site steam methane reforming, SMR). CARB anticipates that, regardless of the rate of H_2 vehicle introduction, most fueling stations will be supplied with LH_2. If a substantial LH_2 infrastructure appears (perhaps alongside a compressed hydrogen infrastructure), then the advanced cryogenic hydrogen storage methods are promising options for high performance storage of hydrogen from LH_2 sources.

The two cryogenic hydrogen storage approaches examined in this paper improve the volumetric density and dormancy of hydrogen storage beyond that available from conventional low-pressure LH_2 dewars, while taking advantage of the thermal insulation techniques developed over the years in conventional LH_2 dewar technology. The first approach, initiated at the Lawrence Livermore National Laboratory (LLNL), is called cryo-compressed storage [10], and seeks to incorporate a high-pressure capability into the cryogenic dewar design, thereby increasing the volumetric storage capacity achieved by high-pressure storage while extending storage times before significant venting of the boil-off gas occurs. The second approach to storing hydrogen is called cryo-adsorption. Recent advances in the materials science and engineering of hydrogen cryo-adsorption materials have been reviewed by Ahn and Purewal [11] and by Johnson and Bénard [12]. Cryo-adsorption is based on the weak binding of H_2 molecules to solids with large surface areas (i.e., usually much greater than 1000 m^2/g) and highly porous structures . Most attention has been focused on activated carbons (AC) and metal organic framework (MOF) compounds, although nanocarbons, zeolites, microporous polymers, and other materials have also been investigated over the past two decades [11][12]. Since adsorption bonding arises from relatively weak van der Waals attractions of the H_2 molecules to the sorbent surfaces, the binding energies are usually about 2–10 $kJ/molH_2$ (in the physisorption range), allowing hydrogen to bind reversibly as a diatomic molecule. However, because the binding of hydrogen is so weak, small increases in temperature lead to desorption, which impedes significantly storage capacities at room temperature. As a result, the sorbent materials need to be cooled to cryogenic temperatures (e.g. $< \sim 100$ K) for significant hydrogen storage capacities to be realized. Since these materials generally have very rapid kinetics for adsorption as well as other potentially attractive properties for hydrogen storage, several systems have been proposed and their thermal performance parameters analyzed for vehicular applications [13].

Recently, Ahluwalia and co-workers [12, 13] conducted an extensive systems analysis study of many types of hydrogen storage systems for light duty vehicles, including well to wheel analysis [4]. Engineered embodiments of both the cryo-compressed and cryo-adsorption methods showed a substantial improvement in the gravimetric and volumetric storage densities of hydrogen when attempting to store 5.6 kg of hydrogen, meeting and exceeding the U.S. Department of Energy (DOE) targets [16].. Cryogenic storage also offers safety advantages. In addition to the cryogenic temperature that minimizes the burst energy in case of an accidental release [17], the design of

cryogenic vessels (pressure vessel encapsulated in a secondary vacuum jacket) provides an extra layer of protection and confinement if the innermost vessel fails. At last, cryo-adsorption materials are not reactive with air, as opposed to many metal hydrides for example.

We present here a comparative analysis of the cryo-compressed and cryo-adsorption hydrogen storage approaches in order to clarify the underlying science of these approaches and to identify specific regimes of temperature and pressure where the two methods are optimal. We review first some basic aspects of the transition between the gaseous and liquid states of hydrogen to better understand the regimes of operation near 20 K, together with a brief review of conventional (low pressure) storage of LH_2 in dewars. The cryo-compressed and cryo-adsorption hydrogen storage methods are reviewed individually, and then explored together, clarifying the materials science and physics of the two approaches in trying to solve the same hydrogen storage task. We hope the discussion is accessible to end users or potential manufacturers needing to assess these hydrogen storage methods for a particular application.

II. Storage of liquid hydrogen in low-pressure dewars and the liquid-gas phase transition

Bowman and Klebanoff recently reviewed the historic methods of storing hydrogen, including low-pressure storage of LH_2 in dewars [6]. Storing hydrogen as a liquid is a clear first approach to increasing both the gravimetric and volumetric storage efficiencies beyond that available from compressed gaseous hydrogen. The volumetric density of liquid hydrogen at its 20 K boiling point is 71 grams per liter, which is nearly twice that of 700 bar compressed gas at room temperature [6]. Still, LH_2 is itself a low-density liquid. For context, the density of water is 1000 g/L, and the volumetric density of hydrogen in water is 111 g hydrogen per liter.

The storage of LH_2 in low-pressure dewars requires specialized vessels that strive to minimize thermal conduction, thermal convection, and thermal radiation associated with the dewar, while also exhibiting mechanical robustness. Unfortunately heat leaks to the cryogenic hydrogen cannot be eliminated entirely, and if storage is intended for extended periods of time, the cryogenic storage vessels must also safely manage the release of the evaporated gas (i.e., boil-off) [18][19][20]. Making matters worse, hydrogen has a remarkably low enthalpy of vaporization (ΔH_{vap}) of only 0.46 kJ/mol, 17.8 times less than that of liquid natural gas (LNG).

Nearly all LH_2 storage vessels use metallic double-walled containers that are evacuated and contain multiple layers of alternating metallic and thermally insulated polymeric or glass films to reduce heat leaks to the cryogenic fluid via convection and radiation. Designs and materials used to construct the containers and all of the components are chosen to minimize thermal conduction. Klell [18] states that most current LH_2 tanks have evaporation losses between 0.3% and 3% per day. The maximum vessel pressure of conventional LH_2 dewars is ~6 bar [3]. The combination of non-zero heat leak rate, low ΔH_{vap} for hydrogen, and low vessel pressure (6 bar) all contribute

to a hydrogen boil-off limitation for conventional dewar storage of LH_2 [4,14]. When the quantities of hydrogen being stored are themselves small, and the storage time between fills is long (weeks), the lifetime of hydrogen in the conventional dewar becomes problematically short.

Consider the fate of a quantity of LH_2, stored in a vessel, and subjected to a heat leak q as shown in Figure 1. The vessel is fitted with a pressure relief device (PRD) such that the pressure in the vessel is always 1 bar or less. LH_2 is placed in the vessel, which is presumed to be precooled such that LH_2 can exist in the vessel for a reasonable amount of time. Initially, the temperature of the LH_2 may be below that of the normal boiling point of 20.3K [19].

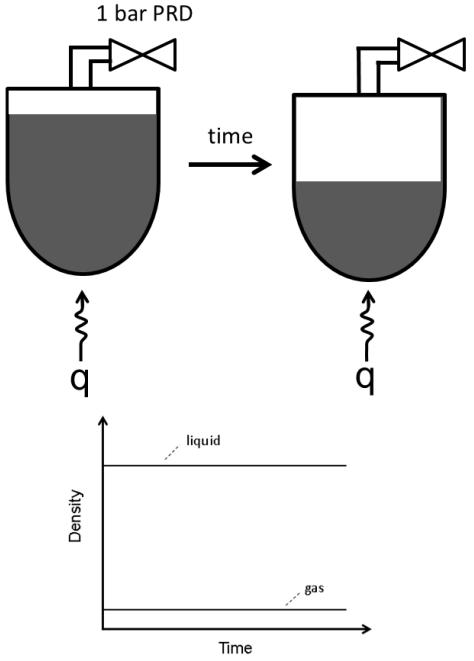

Figure 1. (Top) Evolution of LH_2 in a vessel fitted with a pressure relief device (PRD) set at 1 bar at time=0, subjected to a heat leak q. The darker shading of the liquid phase denotes a higher density than the gas phase (light shading); (Bottom) Variation in the densities of the H_2 gas and liquid phases as the liquid hydrogen evaporates at constant pressure (1 bar)

As the LH_2 is subject to heat leak q with time, the temperature in the liquid will rise, with a concomitant increase in the equilibrium hydrogen vapor pressure above the liquid. The evaporation of hydrogen provides some cooling to the LH_2 since $\Delta H_{vap} > 0$, but as a practical matter such cooling is smaller than practical heat leaks q in cryogenic systems, so the LH_2 temperature continues to rise. When the liquid temperature reaches the normal boiling point of LH_2, the vapor pressure will equal to 1 bar, and "boil-off" begins (time=0 in Figure 1)If the PRD is set to vent just slightly above 1 bar, then as the heat leak progresses, more and more liquid will boil, with the temperature of the liquid holding constant at 20.3K, and the pressure in the vapor maintained at the equilibrium vapor pressure at 20.3K (1 bar). As a result, under the conditions

of Figure 1, the temperature of the liquid phase will remain constant at boiling, and thus the density of the liquid phase remains unchanged as time progresses. Also, since the pressure above the liquid is a constant 1 bar for the conditions of Figure 1, the density of the hydrogen vapor phase remains unchanged at boiling. However, as hydrogen is leaking through the PRD, the heat transfer from the environment vaporizes the liquid hydrogen (dark area at the bottom of the vessel), reducing the amount of liquid hydrogen over time to the benefit of vapor hydrogen. As a result, the quality goes from near 0 (almost all liquid) to near 1 (almost all vapor), even if the densities of both phase remain constant. The boil-off will proceed until there is no liquid hydrogen remaining. At that time, no 2-phase phenomena are taking place and the vapor only hydrogen slowly warms up from 20.3 K to room temperature.

The situation changes dramatically if one now adjusts the PRD to vent at a higher pressure, say 350 bar as might exist for a cryo-compressed storage tank. The situation is shown in Figure 2, where we replace the PRD with a sealed vessel wall rated to the 350 bar pressure of the experiment.

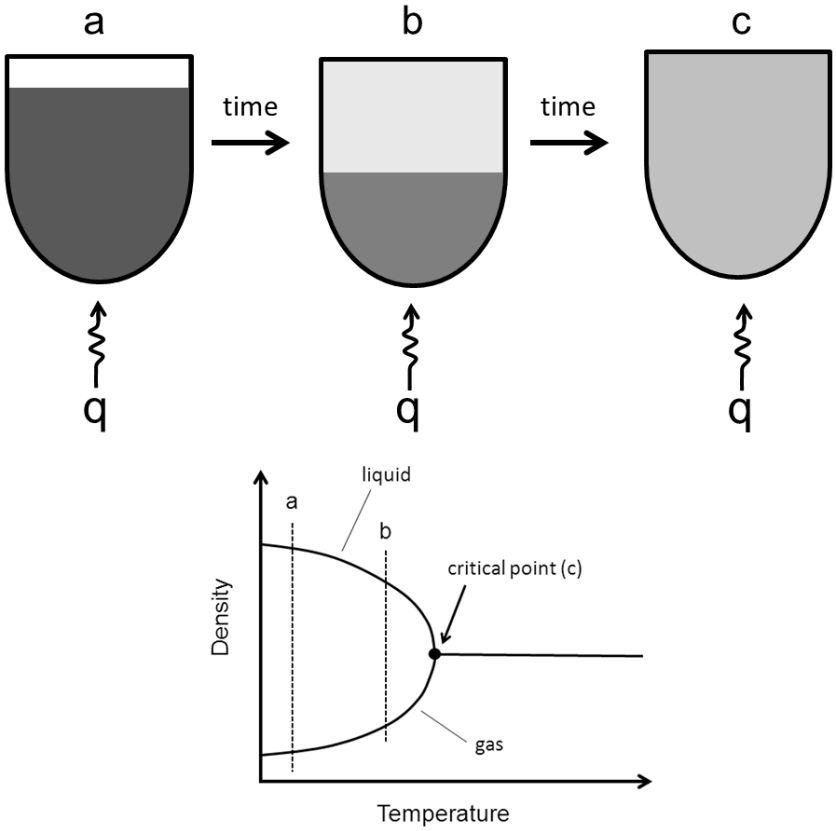

Figure 2. (Top) Evolution of LH_2 in a sealed vessel rated to 350 bar, subjected to a heat leak q. As time progresses, the densities of the LH_2 and vapor components change (indicated by the shadings in a-c.). Darker shading indicates higher density. (Bottom) Schematic of liquid and gaseous densities as a function of temperature (and time) at the critical density (31.3 g/L [22]). The dotted lines "a" and "b"

correspond to the densities depicted in the top pictures a and b, with the top figure c corresponding to the critical point (32.9 K, 12.8 bar [19]) labeled c in the bottom figure.

LH_2 is loaded into the precooled system at an initial temperature of 20.3 K, Figure 2(a).. Since the vessel is sealed, the gas pressure will rise in the system and so will the temperature (ass opposed to Figure 1), increasing the vapor phase density and decreasing the liquid phase density as shown on the bottom of Figure 2. The density of the vapor phase will increase because the pressure is rising with more molecular hydrogen being transferred to the gas phase, and with the temperature rising as well. The shadings in Figure 2 (a) – (c) indicate the density variations in the liquid and vapor phases for this "sealed tank" scenario, with the vapor phase becoming progressively darker, and the liquid phase becoming progressively lighter. Eventually, as the heat leak continues and the temperature rises, the gas phase and liquid phase densities merge to a common value, and the physical distinction between gas and liquid disappears. This point is called the critical point.

The densities of the liquid and gaseous phases for the sealed tank with a heat leak are plotted in a schematic way in Figure 2, bottom. The LH_2 density drops and the vapor density rises, until merging at the critical temperature. Beyond the critical point, only a single "supercritical" phase exists, and with no changes in hydrogen mass in the fixed volume of the tank, the density remains constant as time progresses and the heat leak q continues. As the heating continues, the temperature rises, as does the gas pressure. However, the single-phase gas density remains unchanged, as indicated by the graph in Figure 2.

The critical temperature and pressure are actually unique values (32.9 K and 12.8 bar for para hydrogen) and correspond to a unique critical density (31.3 g/L). Thus, in the entire phase space possible for pressure, temperature and mass of H_2 in the vessel (i.e. density), there is only one special combination of the three such that when the liquid just starts to evaporate, it creates a vapor of identical density. For all other combinations of temperature, pressure and mass of hydrogen, the very first quantities of gas produced by evaporation will have a density lower than the liquid from which it came, producing a discontinuous change in density in going from liquid to vapor (and vice versa).

Thus, we see that the graph of Figure 2 is only applicable for a special case of the vessel where the mass of hydrogen m loaded into the vessel with volume V has a density m/V equal to the critical density 31.3 g/L. For arbitrary densities greater or lower than the critical density, we actually observe discontinuous changes in the density during the first-order liquid-phase transition. These changes are shown in Figure 3 for the critical density of 31.3 g/L, corresponding to Figure 2, along with a higher density situation of 70 g/L and the situation for the lower density of 10g/L.

It is best to discuss Figure 3 coming from the high temperature part of the phase space. If one loads a lot of gaseous hydrogen into the vessel, say 70 g/L, and the system is cooled by some

means, the hydrogen density remains constant (because mass and volume are fixed), and one follows as a single phase the straight line of 70 g/L density shown in Fig 3. Because the density is already high, one can imagine that as the system is cooled to 21 K, the system intersects the liquid density curve first, and the system phase separates, creating a two-phase system characterized by a dense liquid phase with density slightly higher than the starting density of 70g/L, and a much-less-dense vapor phase. The mass of hydrogen contained in the liquid phase would be much larger than the mass of hydrogen existing as vapor when the 70 g/L system phase separates at 21 K, keeping the average hydrogen density at 70 g/L.

Figure 3 also shows the case if one loads a small amount; say 10g/L of hydrogen gas into the vessel starting at elevated temperature. Now, as that system is cooled, the density remains constant and one follows as a single phase flat line of 10 g/L. Because the density starts out low, one can imagine that as the system is cooled to 29.7 K, the system intercepts the vapor density curve first, and the system phase separates, creating a two-phase system characterized by a distinct vapor phase with density slightly lower than 10 g/L, and a much denser liquid phase. The mass of hydrogen contained in the vapor phase will be larger than the mass of hydrogen existing as liquid when the 10 g/L system phase separates at 29.7 K, keeping the average hydrogen density at 10 g/L.

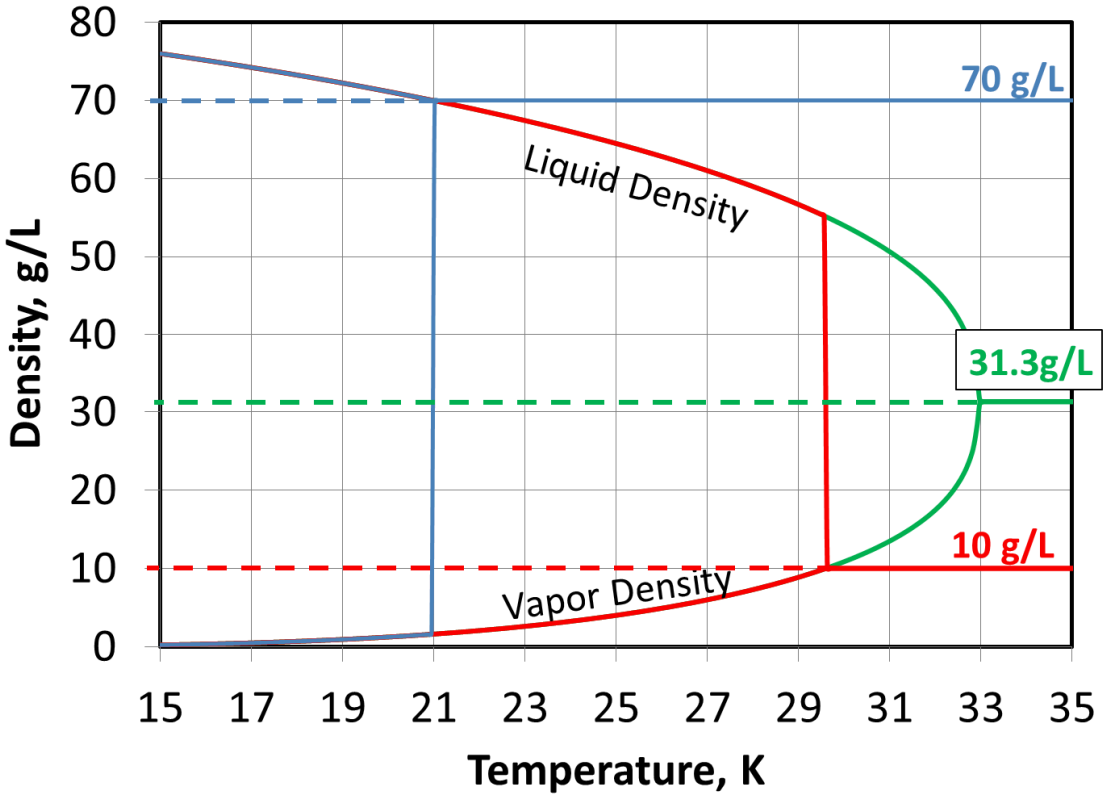

Figure 3. Variation of liquid and vapor densities as a function of temperature for varying densities of hydrogen loaded into the vessel for 3 densities: 70, 31.3 (critical value) and 10 g/L.

Regardless of the initial starting density in Figure 3 (10 g/L, 31.3 g/L or 70 g/L), once the hydrogen gas is cooled to intercept the liquid and vapor density curves, as the system is cooled further, the liquid and vapor phases track their respective density curves in Figure 3. What varies with starting hydrogen density is the mass of hydrogen that exists in either the liquid or vapor phase at any given temperature, as described above.

Taking a continuous family of such horizontal cuts with varying starting density and noting the values of temperature and vapor density (which can be converted to pressure) that are intersected (Figure 3), we can plot the various temperatures and pressures for different starting hydrogen densities that produce simultaneous liquid and vapor phases, termed the "saturation line". The resulting curves are shown in Figure 4.

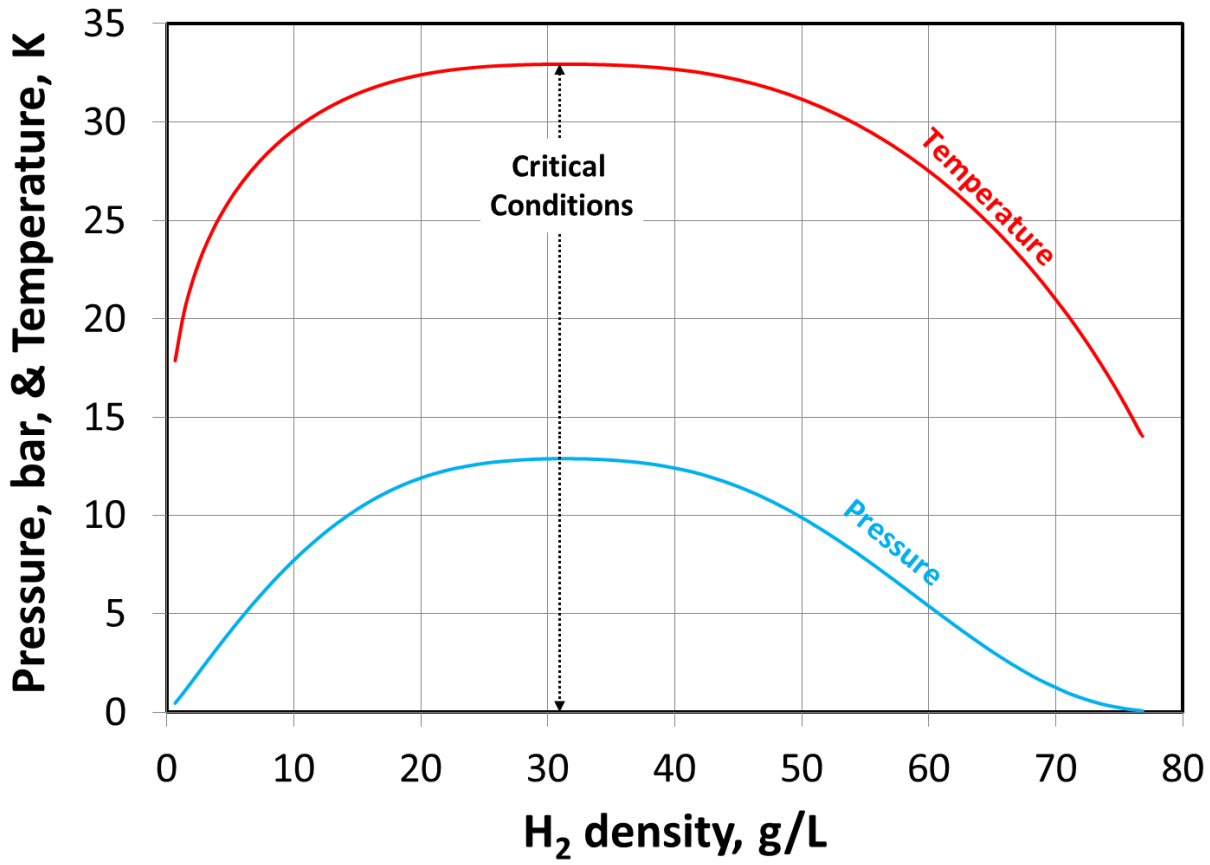

Figure 4. Plot of pressure (bar) and temperature (K) corresponding to liquefaction (co-existence of vapor and LH_2) for various values of hydrogen density. Pressure and temperature share a common ordinate axis, with the different units for pressure and temperature indicated.

One can see that the values of temperature and pressure corresponding to onset of liquefaction vary quite a bit depending on the original hydrogen density loaded into the system. The graph in

Figure 2 applies for the special case where the mass of hydrogen loaded in the vessel corresponds to the critical density.

For the cryogenics technologies that will be discussed, the system exists most of the time in the one-phase "supercritical" region beyond the critical point. As such, the hydrogen for the most part exists only as a one-component cold gas, with properties describable by a real gas equation of state for hydrogen, such as the 32 term modified Benedict-Webb-Rubin equation [22].

III. Hydrogen storage by cryo-compression

Cryo-compressed storage systems, abbreviated CcH_2, were originally developed in response to the main drawback of storing hydrogen in conventional LH_2 dewars: boil-off. Cryo-compression consists of storing hydrogen at cryogenic temperatures and at high pressure in a high-pressure vessel so that dormancy (defined as the period of inactivity before a vessel releases H_2 to reduce pressure build-up) can be greatly improved [23]. A cryo-compressed storage system consists of a composite pressure vessel with a metallic liner that is encapsulated in a secondary insulated jacket, whose role is to limit heat transfer between the hydrogen and the environment (see Reference [24] for more details, where a cryo-compressed system operating at a maximum pressure of 345 bar has been demonstrated with a full scale 151 L internal volume, 10.4 kgH_2 vessel installed onboard a type 1 Toyota Prius). A schematic design of a cryo-compressed storage tank is shown in Figure 5.

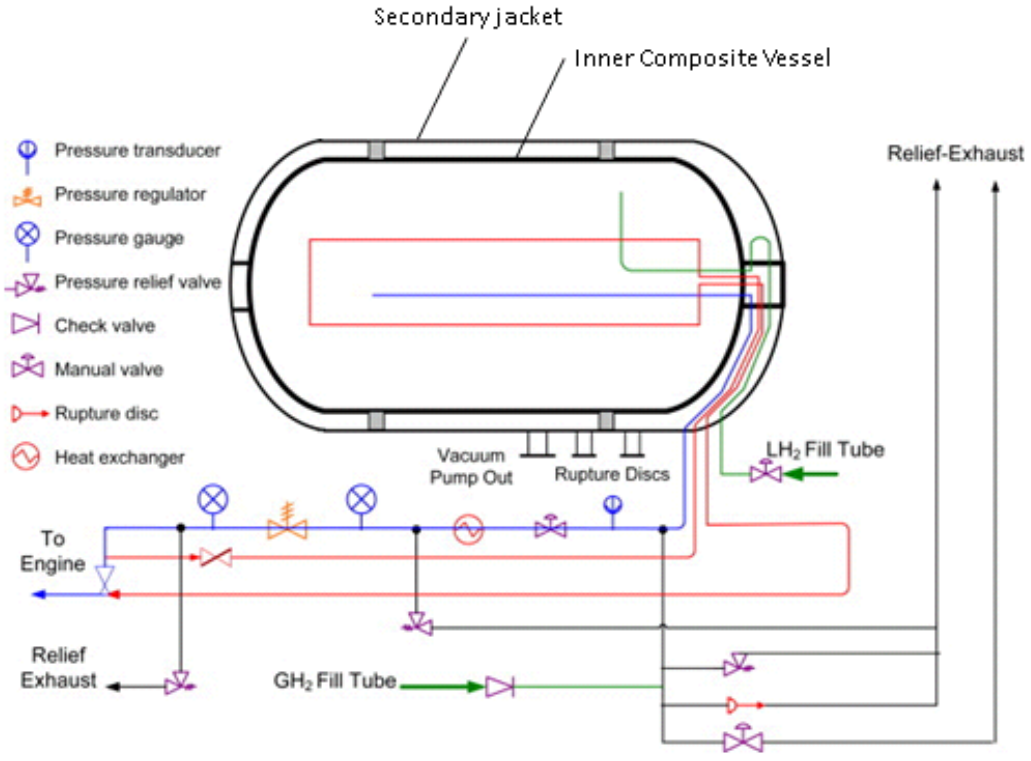

Figure 5. Design schematic of a cryo-compressed H_2 storage system. Figure reproduced with permission from Ref. [15].

Figure 6 provides a comprehensive presentation of the thermodynamic behavior of CcH_2 systems, enabling computation of at least the 2 major phenomena of particular interest to the end user: parking (or dormancy), computed through absorbed energy, and driving, computed though constant entropy lines (hydrogen extraction is considered to be reversible and adiabatic for the vessel). Figure 6 uses axes of specific internal energy and density instead of more traditional temperature and pressure. An appropriate choice of scales radically simplifies dormancy calculations. The grid scale in the specific internal energy (horizontal) axis is set at 86.4 kJ/kg H_2, which converts to 1 Watt-day/kg H_2. The grid scale in the mass (vertical) axis represents 1 kg H_2. Therefore, the area of a grid rectangle represents 1 Watt-day of heating. The total change in internal energy (in Watt-days) can be easily calculated by counting rectangles under the curve representing changing the state of hydrogen from one point to another in Figure 6. Dormancy (days) is calculated by dividing the internal energy change (in Watt-days) by the rate of heat transfer (in Watts).

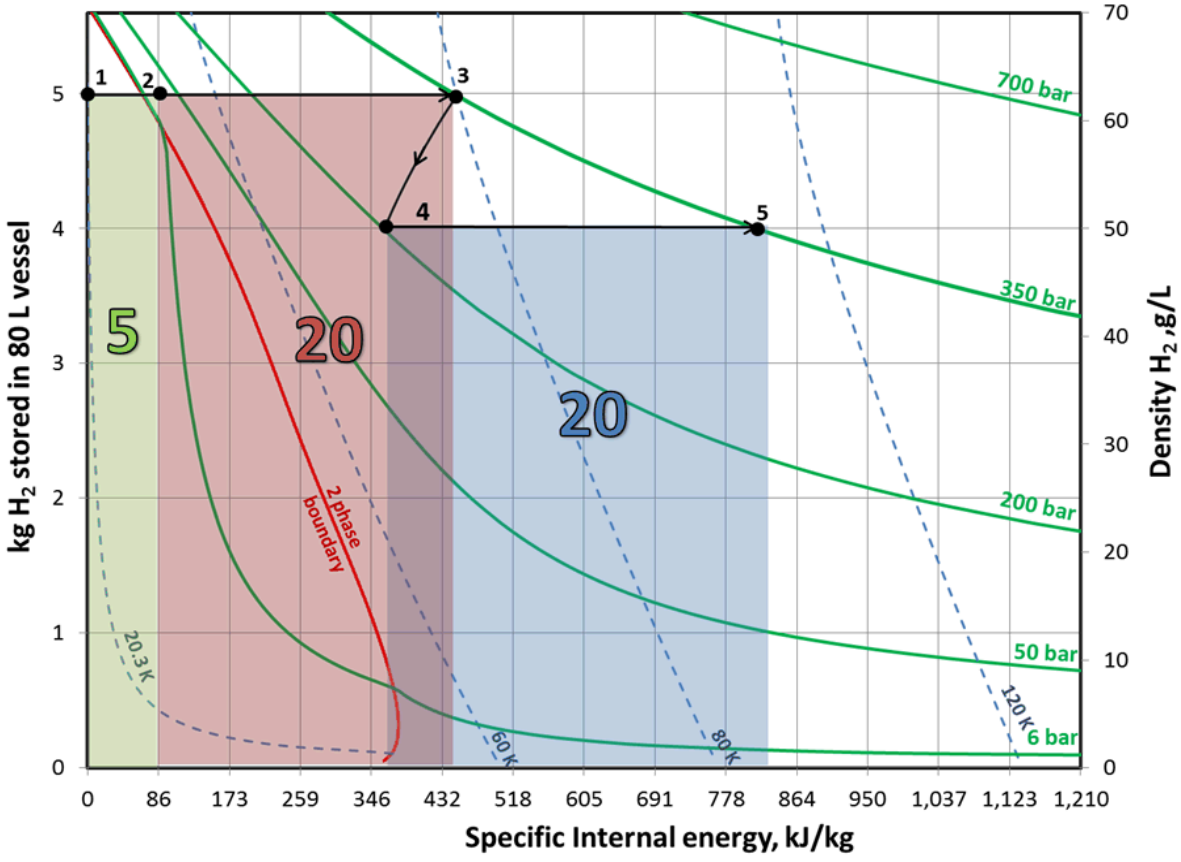

Figure 6. Phase diagram for H_2 showing density (right vertical axis) and specific internal energy (horizontal axis), with lines for constant pressure (solid) and temperature (dashed). Curves for entropy are not shown. The left axis shows the mass of H_2 contained in a vessel with 80-liter internal volume, which

would store 5.6 kg of LH_2 at 20 K and 1 bar. The figure also shows points and areas representing dormancy (in Watt-days) of conventional LH_2 tanks (green) and cryogenic pressure vessels (red and blue). Dormancy (days) is calculated by dividing the internal energy change (in Watt-days) by the rate of heat transfer (in Watts). Figure reproduced with permission from Reference [23].

A dormancy calculation begins by identifying the initial thermodynamic state in Figure 6 of the H_2 contained in the vessel. As an illustration, consider a parked automobile with a conventional low-pressure LH_2 dewar with 80 L internal volume and 6 bar maximum working pressure, which is 90% full with 5 kg LH_2 at 20 K and 1 bar (point 1 in Figure 6). As the vehicle is parked (not using H_2), heat transfer from heat leaks warms the H_2 increasing the internal energy and with it, both the temperature and pressure. Dormancy ends in this case when the pressure reaches 6 bar (Point 2), when H_2 venting or vehicle driving becomes necessary to maintain pressure within the vessel rating. Total heat absorbed during this process from point 1 to point 2 can be calculated by counting the number of rectangles (5 Watt-days) in the area marked in green. Dormancy can then be calculated by dividing 5 Watt-days by the heat transfer (i.e. heat leak) rate. If one has a heat leak rate of 4 Watts total, then the dormancy would be 1.25 days before loss of hydrogen.

In progressing from point 1 to point 2, the system crosses the red line in Figure 6 termed the "2-phase boundary." This line denotes points of mass (density) and internal energy (or temperature) where distinct and separate liquid and vapor phases exist in equilibrium with each other (saturation line). Such points correspond to the vapor and liquid density curves shown previously in Figures 2 and 3. Point 1 in Figure 6 corresponds to a state of almost zero internal energy where the hydrogen exists almost exclusively as a liquid, with very little hydrogen in the vapor state. With heat leak, the system establishes a liquid-vapor equilibrium upon intersecting the red 2-phase boundary line. Further heating takes the system to point 2, which corresponds to a single supercritical fluid phase. As will be discussed the remaining points 3 – 5 involve the system being in a single (but cold) vapor phase of the system.

Figure 6 illustrates the dramatic increase in dormancy of hydrogen storage when the pressure limit of the cryogenic vessel is increased, say to 350 bar. An auto initially filled with 5 kg LH_2 at 1 bar and 20 K can accommodate a heat leak while parked until the pressure reaches 350 bar (Point 3 in the figure) without venting any H_2. Counting rectangles under the line joining Point 1 and Point 3 (two shaded regions) we obtain 5+20=25 Watt-days, *five times* greater thermal endurance than a conventional LH_2 tank.

Furthermore, unlike conventional LH_2 vessels, cryogenic pressure vessels dramatically extend dormancy as the vehicle is driven. For example, if the parked vehicle is driven when the H_2 is at point 3 (Figure 6), consuming 1 kg of H_2 fuel, the remaining H_2 in the vessel expands and cools following a constant entropy line from point 3 to a point of lower hydrogen density, point 4. If the vehicle were not driven further, the heat leak would drive the system from point 4 to point 5, extending the vessel thermal endurance by an additional 20 Watt-days. Eventually, venting will

occur at point 5 as the internal pressure exceeded the 350 bar pressure limit of the vessel. In this way, periodic driving substantially extends dormancy, essentially eliminating fuel loss for even very moderate driving patterns. Dormancy can be increased by either improving insulation (reducing heat leaks) or by strengthening the vessel (raising the vent pressure).

Figure 6 is somewhat conservative because it neglects secondary effects such as vessel heat capacity and heat potentially absorbed by conversion between the two states of nuclear spin arrangement (i.e., *para*-H_2 conversion to *ortho*-H_2) of H_2 molecules [25]. Both of these effects divert heat flow away from the internal energy of the stored hydrogen, thereby increasing the dormancy of the vessels.

IV. Storage of hydrogen by cryo-adsorption.

The volumetric storage density of light gases such as hydrogen can be increased significantly by exploiting the attractive forces between hydrogen and other atoms. As mentioned above, a given volume of water contains more hydrogen than the same volume of liquid hydrogen. Hydrogen can be stored through chemical binding to other elements in complex metal hydrides [26], chemical hydrides [27], inside a solid metallic matrix as atoms in interstitial metal hydrides [28] or by chemisorption or physisorption on large surface area materials [11], [12]. Here we focus on physisorption of molecular hydrogen on large surface area materials at cryogenic temperature, an approach called cryo-adsorption.

When molecular hydrogen encounters a weakly binding physisorption solid surface, there is an attractive interaction due to van der Waals forces between the hydrogen molecule and the surface, and the surface of the substrate can become covered with adsorbed molecular hydrogen. The molecular hydrogen represents the "adsorbate" while the solid surface constitutes the "adsorbent". The desorption enthalpy ΔH_{des} is the change in enthalpy in going from the physisorbed state to the free gas-phase state and is typically positive, meaning that the adsorbed state has lower energy than the unbound state.

This desorption enthalpy is a determining factor in the thermodynamic description of the behavior of cryo-adsorption-based storage, sets the energy scale required for charging and discharging hydrogen, regulates the thermal behavior and sets boil-off rates for cryogenic adsorption systems. Cryo-adsorption materials (also called "sorbents"), with desorption enthalpies greater than 50 kJ/mol H_2 require more energy to release 5 kg of hydrogen than that required to boil the equivalent mass of water [6]. On the other hand, materials with ΔH_{des} values smaller than 10 kJ/mol H_2 require cryogenic temperatures to achieve acceptable storage densities, and can be released using heat from the environment. The hard-to-achieve range ΔH_{des} = 10 - 30 kJ/molH_2 is believed to be optimal for materials-based hydrogen storage applications, depending on the entropy change for the process. For the cryo-adsorption material discussed here, the ΔH_{des} values are ~ 5kJ/mol H_2 to 15 kJ/mol H_2.

The physical concept of a surface, in highly microporous crystals such as MOFs, can sometimes be hard to define. The surface can be formally defined as the geometric structure produced by rolling a probe molecule over the microporous framework at a distance corresponding to the strongest adsorbate-adsorbent interaction. The adsorption process occurs within the porous structure of the adsorbent, which is the volume of the adsorbent externally accessible to the adsorbate molecules. The pores of the adsorbents are formally classified as micropores (pore size less than 2 nm), mesopores (2 - 50 nm) and macropores (larger than 50 nm). In order to optimize gas-surface interactions, gas storage applications of the adsorption phenomena usually require maximizing the microporous volume of an adsorbent. The adsorption effect represents a local enhancement of the density of the adsorbate close to the adsorbent surface resulting from the attractive interactions, as shown in Figure 7.

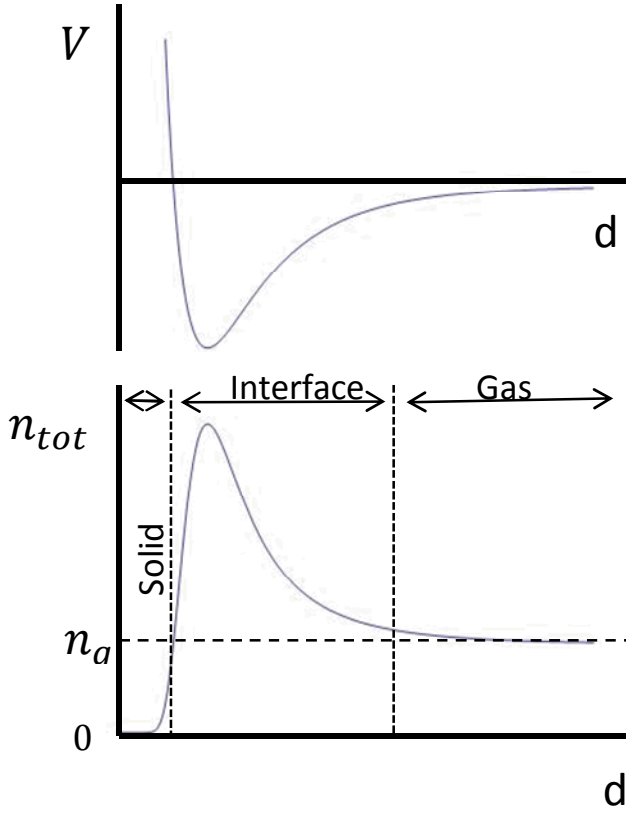

Figure 7. (Top): Distance dependent potential experienced by a gas close to a cryo-adsorption surface. (Bottom): Density profile of a gas close to an adsorbing surface. The enhanced density in the vicinity of the adsorbent is caused by attractive gas-surface interactions (top figure). The gas/interface boundary indicated on the bottom figure depends on the definition of a cut-off for the interaction potential. Molecules within the interface region are considered to be adsorbed.

Given a microporous cryo-adsorption material with a reasonable ΔH_{des} value such as activated carbon, a cryo-adsorption tank for storing hydrogen can be conceived as shown in Figure 8. The cryo-adsorption tank contains internal heat exchange hardware (fins) that contact the powdered

sorbent material and the tank can is designed to have LN_2 flow through the internal fins to pre-cool the cryo-adsorption material as hydrogen (in the form of LH_2) is flowed into the tank.

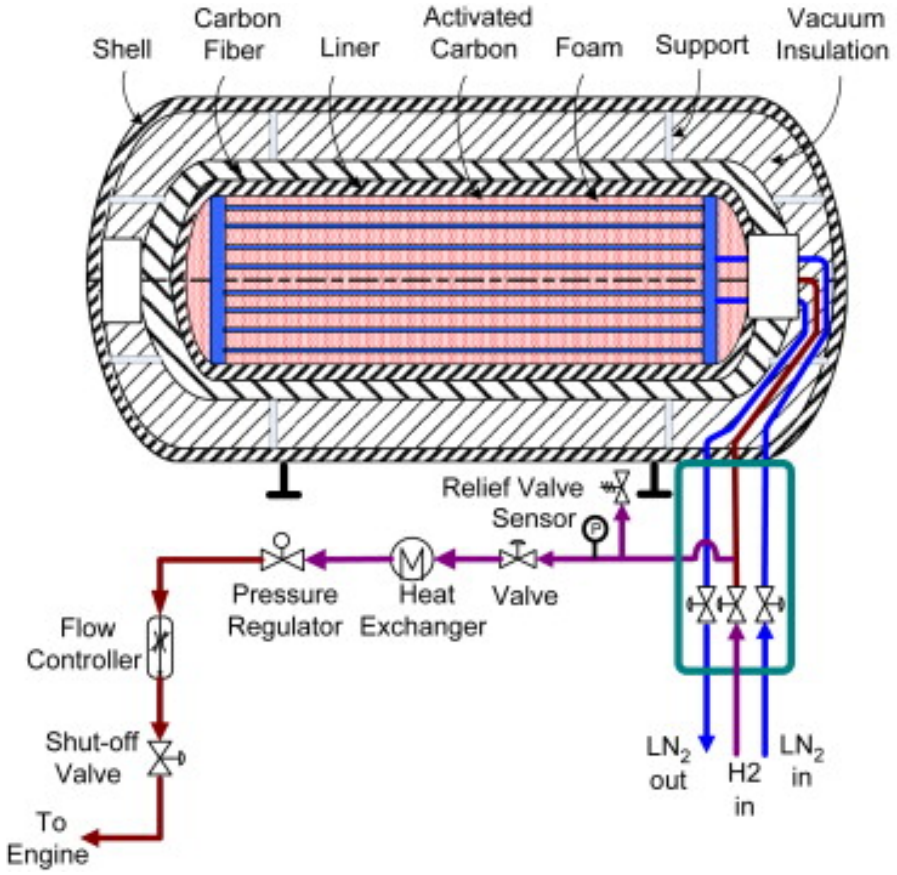

Figure 8. Schematic of a complete system for the reversible storage of hydrogen via adsorption on activation carbon. Figure reproduced with permission from Reference [29].

The hydrogen adsorption process is characterized by an equation of state: the adsorption isotherm. The adsorption isotherm is usually defined in the Gibbs sense as the difference between the mass of hydrogen bound to the porous structure and the mass of hydrogen that would be present in the same volume if the porous material were not there [6,7]. The Gibbs adsorption isotherm is also called the excess adsorption isotherm, as it refers to the gain in density over that prevailing at the equilibrium pressure established for a given temperature. The absolute adsorption isotherm refers to the total amount of hydrogen present within the potential field of the adsorbent (i.e. within the interface region of Figure 7), which corresponds to the volume of the adsorbed phase.

Obtaining the absolute adsorption isotherm from the excess requires knowing the volume of the adsorbed phase, which is not directly accessible experimentally and depends very much on the definition of a cut-off of the adsorbate/adsorbent interaction potential. For microporous adsorbents, in which most of the volume of the pores is subject to the interaction potential, the

absolute adsorption isotherm corresponds to the total uptake of adsorbate inside the pores. However for mesoporous and macroporous adsorbents, adsorbate molecules far from the adsorbent surfaces (yet still inside the meso- or macro-pore) should be excluded. An unambiguous definition of the absolute adsorption isotherm can therefore be difficult, particularly for adsorbents with a complex pore size distribution. The excess adsorption isotherm represents, however, a clear, experimentally accessible concept [6].

The total density of adsorbate molecules in a porous structure with a pore size distribution that includes mesopores and macropores can be referred to as the stored density of adsorbate in the adsorbent. The excess adsorption isotherm for the candidate cryo-adsorption material AX-21 is shown in Figure 9.

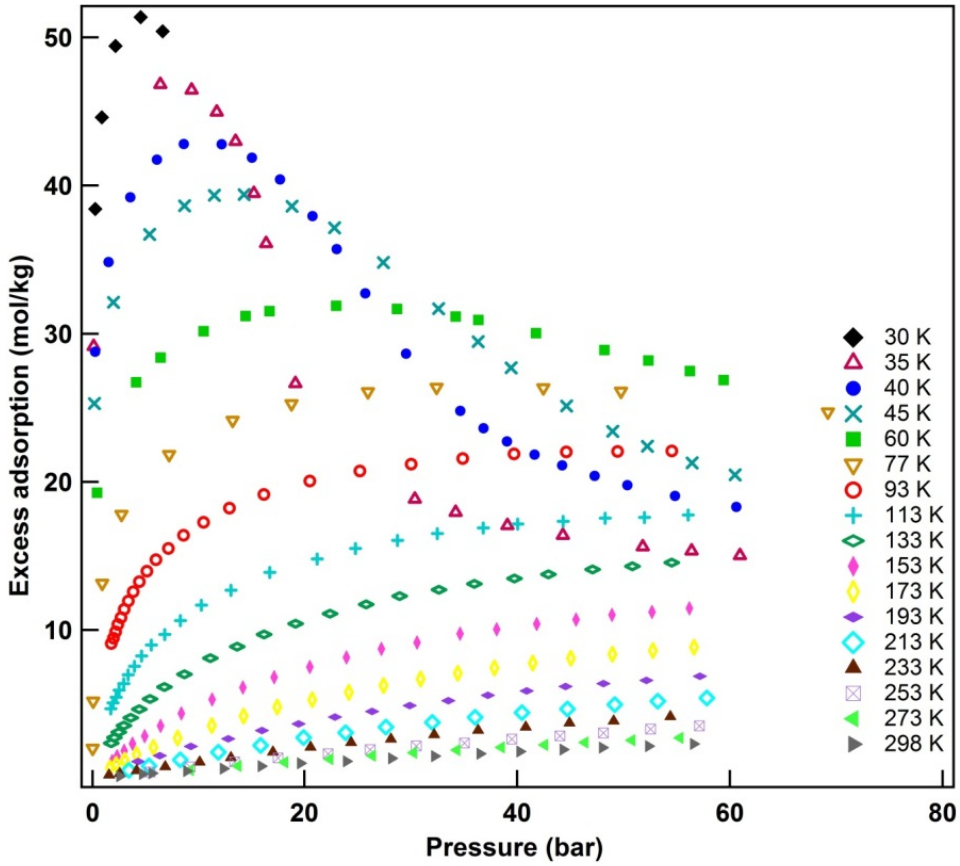

Figure 9. Excess adsorption isotherms of hydrogen on the activated carbon AX-21 as a function of pressure for several temperatures (experimental measurements from Reference [27]).

One can see that the greatest excess hydrogen density in the microporous material AX-21 is achieved by going to low pressure and low temperatures. At its peak, ~ 50 mol of hydrogen (100.5 g) of hydrogen are adsorbed in excess within the material at 5 bar and 30 K. However,

this excess hydrogen required 1 kg of adsorption material, so there is a significant weight penalty associated with the excess hydrogen density gain afforded by cryo-adsorption.

Due to the adsorbate-adsorbent interactions, the total density of H_2 in the porous structure of the adsorbent can become larger than the liquid density of hydrogen at its normal boiling point. For both MOF-5 and CuBTC, at temperatures below 50 K and for pressures above 127 bar, densities about 20% greater than that of LH_2 at its boiling point can be achieved despite being above critical point. Physical adsorption on microporous adsorbents has been widely used for the separation and purification of gas mixtures [28, 29]. The adsorption phenomena, through gas surface interactions, also offers the possibility of substantially lowering the storage pressure of gases, such as natural gas and hydrogen [28, 29].

The recoverable stored hydrogen density is defined as that amount of gas stored that can be practically recovered from the storage system by reducing the pressure isothermally to the minimum operating pressure of the fuel cell. If the cryo-adsorption tank of Figure 8 connected to a PEM fuel cell that requires at least ~ 3 bar to operate properly. The recoverable density is the amount of gas delivered to and consumed by the PEM fuel cell. The recoverable density is the total amount of hydrogen stored in the cryo-adsorption tank minus the amount of hydrogen which remains in the tank at the pressure below which the fuel cell can't operate.

The residual hydrogen density can be substantial at low temperatures for cryo-adsorption systems due to binding of hydrogen molecules to the sorbent at low temperature. This bound hydrogen can be recovered by heating the system using heat from the environment by allowing the temperature of the reservoir to rise during discharge (passive storage system) or by using heating wires (active storage system). Alternatively, the waste heat from the fuel cell can provide this source of energy.

We now describe our approach to the comparative analysis using a common thermodynamic formalism.

V. Thermodynamic modelling of the cryo-compression and cryo-adsorption hydrogen storage methods

At the highest level we are interested in how much hydrogen can be stored in a given internal volume at some temperature and pressure for the CcH_2 and cryo-adsorption approaches. The total mass m_{tot} of H_2 (adsorbed and not-adsorbed) that one can store in a cryo-compression or cryo-adsorption hydrogen storage vessel of volume $V_{internal}$ is given as the sum of the two terms:

$$m_{tot} = m_g + m_a = (V_{internal} - m_s V_a - V_s)\rho_g + m_s M_{H_2} n_a \qquad (1)$$

The mass m_{tot} represents the total mass of hydrogen in the system. The subscript "g" refers here to hydrogen molecules that are not adsorbed, existing instead in the gaseous, liquid or supercritical states. The term m_s is the mass of the cryo-adsorption material. The subscript "a"

refers to molecules of hydrogen that are actually adsorbed in the sorbent material, constituting the absorbed "excess" described previously. For the cryo-compression case, we have $m_s = 0$. Tables 1 and 2 define the variables of equations (1) to (5).

The total internal volume $V_{internal}$, where any hydrogen molecules and the sorption material are contained, is the sum of the volume of the skeleton V_s of the sorbent (whose density is similar that of graphite $\rho_c \sim 2.2$ kg/L [30]) and the total void volume $V_{void}\, m_s$. The void volume V_{void} is generally described per unit mass of adsorbent substrate and is the sum of the volume of the gaseous phase V_g and the adsorbed phase V_a:

$$V_{internal} = V_{void} m_s + V_s = (V_g + V_a) m_s + m_s/\rho_c \qquad (2)$$

Table 1. Definition of variables in Equations 1 to 5.

Variable	Definition
h_{in}	Enthalpy of hydrogen gas incoming, [kJ/kg]
h_{out}	Enthalpy of hydrogen gas exiting, [kJ/kg]
m_{Al}	Mass of the aluminum liner, [kg]
$m_{composite}$	Mass of the composite wall, [kg]
m_g	Mass of H_2 not adsorbed, [kg]
$\dot{m}_{in}$	Mass flow of H_2 into the tank, [kg/s]
M_{H_2}	Molar mass of H_2, [kg/mol]
$\dot{m}_{out}$	Mass flow of H_2 out of the tank, [kg/s]
m_s	Mass of sorbent material, [kg]
m_{tot}	Total mass of hydrogen in both adsorbed and not adsorbed phases, [kg]
n_a	Moles of excess H_2 absorbed on sorbent, given per mass of sorbent, [mol/kg]
Q	Heat transfer between H_2 storage tank and environment, [kW]
q_{st}	Isosteric enthalpy of adsorption, [kJ/mol]
ρ_g	Density of H_2 not absorbed on sorbent, freely moving in the vessel, [kg/m^3]
U_g	Internal energy of H_2 not absorbed on sorbent, [kJ]
U_a	Internal energy H_2 absorbed on sorbent, given per mass of sorbent, [kJ/kg]
U_{Al}	Internal energy of the aluminum liner, [kJ/kg]
$U_{composite}$	Internal energy of the composite, [kJ/kg]

U_s	Internal energy of sorbent, [kJ]
U_{tank}	Internal energy of storage tank due to the heat capacity of the wall, [kJ]
V_a	Volume of the adsorbed phase, given per unit of mass of sorbent, [m^3/kg]
$V_{internal}$	Internal volume of the vessel where sorbent and H_2 are stored, [m^3]
V_g	Volume of the gaseous phase, given per mass of sorbent, [m^3/kg]
V_s	Volume of the substrate skeleton, [m^3]
V_{void}	Void volume, given per mass of sorbent, [m^3/kg]

Table 2. Expressions of selected parameters in Equations 1 to 5.

Parameter	Expression
m_s	$V_{internal}\rho_{sorbent}$
n_a	$n_{max}\exp\left[-\left(\frac{RT}{\alpha+\beta T}\right)^2 ln^2\left(\frac{P_0}{P}\right)\right]$
U_a	$-\frac{n_{max}\alpha\sqrt{\pi}}{2}\left[1-Erf\left(\sqrt{\ln(n_{max}/n_a)}\right)\right]+n_a(RT+q_{st}+u_0)$
q_{st}	$-\alpha\sqrt{\ln(n_{max}/n_a)}$
U_s	$\frac{m_s(38+3/2\,T)}{1000}T$
U_{tank}	$m_{Al}U_{Al}+m_{composite}U_{composite}$

The thermodynamic state of the not-adsorbed phase of hydrogen is derived from the 32-term modified Benedict-Webb-Rubin expression for the real gas equation of state for hydrogen [19]. The cryo-adsorption phenomena has been reported to be accurately described over a wide range of temperatures and pressures and for various sorbent materials by the modified Dubinin-Astakhov (D-A) model ([30], [31], [32]). This model will be used throughout this paper. The thermodynamic expressions from the modified D-A model are reported in Table 2 (n_a, U_a). The isosteric enthalpy of adsorption q_{st} is also given here for reference. We refer the reader to the original literature for a full discussion of the various parameters defining the modified D-A model for cryo-adsorption [31].

Table 3 summarizes the D-A parameters of various sorbents found in the literature: n_{max} (saturation density of the isotherm), P_0 (saturation pressure), α (constant energy parameter to the Dubinin characteristic energy U_a), β (coefficient of the linear correction term to the Dubinin characteristic energy), V_a (volume of the adsorbed phase) and the sorbent density $\rho_{sorbent}$.

Table 3. Modified D-A parameters of sorbents considered for H_2 storage

parameters	*Units*	**CNS-201**	**$Cu_3(BTC)_2$**	**AX-21**	**powder MOF-5**	**compacted MOF-5**	**MIL-101**
n_{max}	*mol/kg*	24.5	34.7	71.6	88	74.9	69.5
P_0	*MPa*	2110	1290	1470	296	357	714
α	*J/mol*	4750	4430	3080	2490	2430	2680
β	*J/mol/K*	16.7	14.1	18.9	11	11.5	15.5
V_a	*L/kg*	0.485	0.648	1.43	1.9	1.57	1.2
$\rho_{sorbent}$	*kg/L*	0.34	0.46	0.3	0.15	0.51	0.45[1]
Reference		[30]	[30]	[31]	[33]	[34]	[35]

Table 4. Gravimetric specific surface of sorbents considered for H_2 storage

parameters	*Units*	**CNS-201**	**$Cu_3(BTC)_2$**	**AX-21**	**powder MOF-5**	**compacted MOF-5**	**MIL-101**
A_s	m^2/g	1440	1570	2800	2762	2300	2761
Reference		[30]	[30]	[31]	[36]	[36]	[37]

The optimal operating conditions (pressure and temperature) for adsorption-based hydrogen storage systems have yet to be clearly defined. They are of course also a function of the properties of each material. Kumar et al [38] published a system simulation for AX-21 at a pressure of 35 bar and a temperature of 77 K. Richard et al [30] proposed a maximum cryo-adsorption tank pressure of 350 bar and temperatures down to 60 K. Chakraborty and Kumar [39] studied thermal management for cryo-adsorption systems of 60 and 200 bar, at 80 K, for AX-21 and MOF-5. Hardy et al [40] reports a similar design at 200 bar for MOF-5. Purewal et al [36] investigated pressure effects up to 100 bar at 77 K for MOF-5. More recently, Tamburello et al [33] proposed a 100 bar and 80 K design for powdered MOF-5.

Figure 10 predicts the intrinsic stored hydrogen densities ($m_{tot}/V_{internal}$) that can be achieved with the CcH_2 and cryo-adsorption methods, without any consideration of tankage, internal heat

[1] Bulk density from MIL-101 is taken from [32]. It is assumed there is no space between pellets, e.g., pellets are cubic or hexagonal uniformly compacted without breaking down the atomic structure of the unit cell of the solid. A bulk MIL-101 density of 0.45 kg/L is chosen instead of 0.47 kg/L to make up for the sharp dropdown of excess hydrogen adsorption that has been observed for this material.

exchangers, or any other balance of plant item. The densities are associated with the physical system itself, cold hydrogen fluid in the case of cryo-compressed, and a combined system of cold fluid and cold adsorbent in the case of the cryo-adsorption system. The total H_2 density is plotted as a function of pressure for three temperatures: 40, 77 and 150 K, assuming an inner volume completely filled with cryogenic adsorbent at its given density.

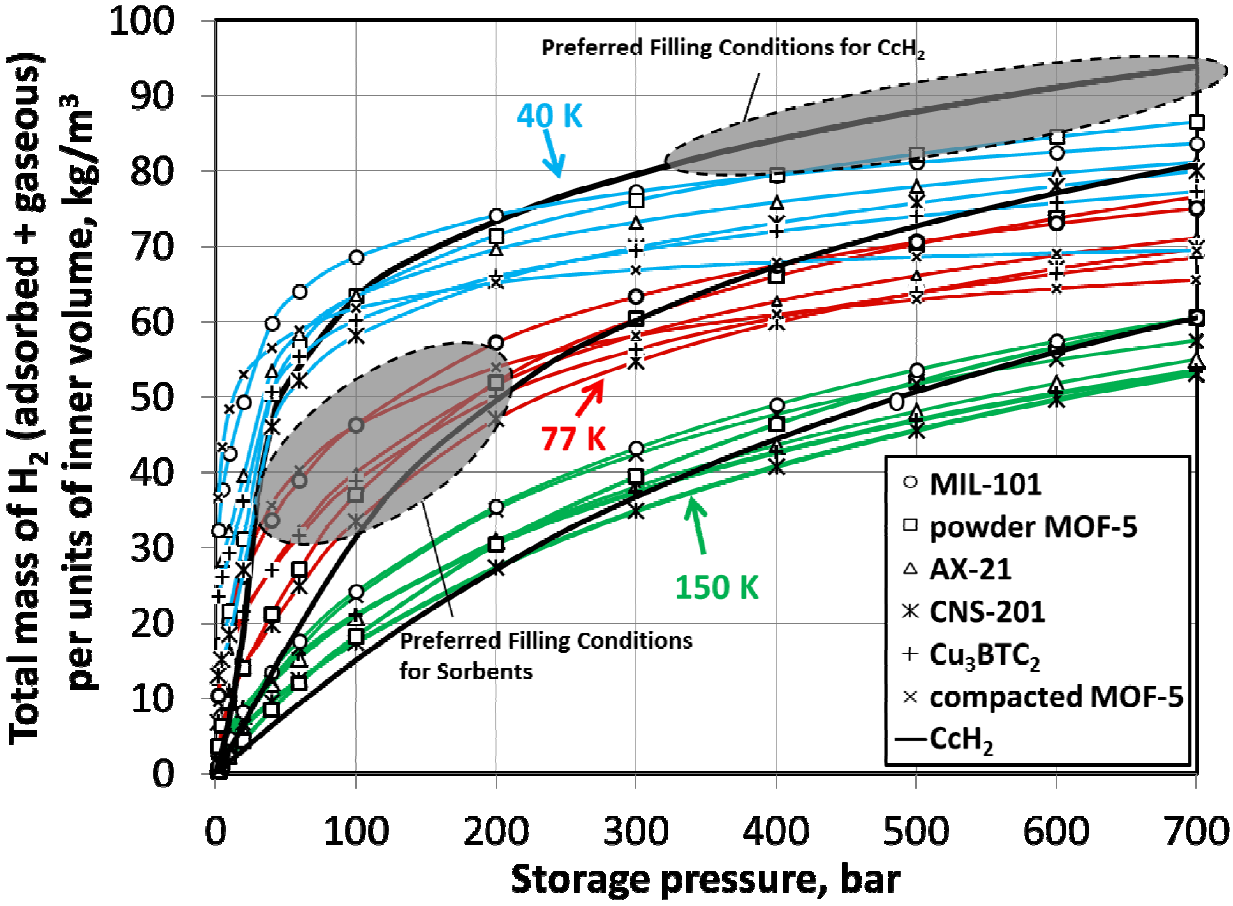

Figure 10. Total H_2 density (including both adsorbed and gaseous phase) for the cryo-adsorbents listed in Table 3 as a function of pressure for 3 temperatures (40, 77 and 150 K), calculated from Equation (1) per unit of internal volume using the modified D-A model (Tables 2 and 3). The densities for the CcH_2 approach are also reported (black continuous lines). The typical preferred filling conditions for each approach are shaded in gray. The inner volume is completely filled with cryogenic adsorbent at its given density.

Figure 10 enables one to map the conditions of temperature and pressure for the optimal use of CcH_2 and cryo-adsorption methods in terms of stored H_2 capacity (or density). At first, we see that the density is an increasing function of the storage pressure for all cases, and that this effect increases with decreasing temperature. The largest difference between the sorbent materials and the cryo-compressed case appears to be around 100 bar and 77 K, where the stored density of MIL-101 and compacted MOF-5 is 50% higher than for CcH_2 (45 versus 30 kg/m^3). The

presence of the cryo-adsorbent promotes density by virtue of the surface hydrogen excess in the adsorbed layer. The ordering of the mass density for the different sorbents at 77 K and 100 bar is: MIL-101 > compacted MOF-5 > AX-21 > Cu_3BTC_2 > powder MOF-5> CNS-201>CcH_2. At 40 K and 350 bar, it becomes: CcH_2>MIL-101 > powder MOF-5> AX-21 > CNS-201> Cu_3BTC_2 > compacted MOF-5**.** Except for powdered MOF 5 and CNS 201, this ordering generally correlates with the specific surface area per unit volume of the adsorbents, which can be calculated from the product of their gravimetric specific surfaces (A_s – see Table 4) and their density ($\rho_{sorbent}$) : 1458.45 m^2/cm^3 for MIL-101, 1173 m^2/cm^3 for compacted MOF 5, 840 m^2/cm^3 for AX-21, 722 m^2/cm^3 for CuBTC, 359 m^2/cm^3 for MOF 5 powder, and 490 m^2/cm^3 for CNS 201. The relative benefit of the presence of a sorbent material reduces with increasing pressure and decreasing temperature. Not including these sorbent materials at pressure larger than 230, 410 and 700 bar (at 40, 77 and 150 K, respectively) enables larger H_2 densities. This detriment arises because the internal skeletal structure of the cryo-adsorption materials takes up space without providing a surface for hydrogen binding, thereby eliminating volume that could otherwise be occupied by dense cold gas. As a result, the preferred operating pressure for these sorbents is less than ~ 250 bar, a regime that takes advantage of the density benefit afforded by the cryo-adsorbent before the volume-exclusion density penalty becomes too large. The optimal fill pressure for the CcH_2 tank is as large as its pressure limit allows.

Another thermodynamic property to consider when studying the influence of sorbent materials is the energy absorption capacity. This is usually considered in the context of a tank with a pre-set maximal vent pressure, as discussed in Figures 1 and 2, and the answer is usually given in terms of dormancy: the time or energy for which the system can sustain the heat leak until the maximal system pressure is reached. Dormancy energy is conveniently expressed in Watt-days (1 Watt-day = 86,400 Joules), so that if we assume a constant heat transfer rate Q (in Watts), then we can directly know the dormancy in days (time of parking before reaching rated pressure) by dividing the Watt-days value by Q. If we consider the change of the internal energy only of the H_2 molecules for the non-absorbed (i.e., gaseous, g) (ΔU_g) and adsorbed (ΔU_a) states, we can calculate the dormancy energy between an initial and a final state (maximum operating pressure) of a constant mass of H_2.

$$\Delta U_{\text{Dormancy}} = \Delta U_{g}{}_{initial}^{final} + \Delta U_{a}{}_{initial}^{final} \qquad (3)$$

At equal conditions (same total mass of H_2 stored, same internal volume, same initial temperature and same venting pressure), the presence of the sorbent material enables the sorbent based storage system to have a greater dormancy than the cryo-compressed system. This is due partly to the isosteric enthalpy of desorption which is endothermic. As the heat leak Q proceeds and the temperature increases, pressure increases as well, but not so quickly since energy is diverted to overcoming the hydrogen desorption enthalpic barrier associated with the adsorbed hydrogen layer.

Figure 11 reveals the dormancy distribution (in Watt-days) between the non-adsorbed and adsorbed H_2 phases for the sorbent materials previously identified, considering a 190 L internal volume, 100 bar vessel filled with 5 kg total of H_2 initially at 80 K. Initial pressure and final temperature are also given, which vary since the sorbent materials have different stored hydrogen densities under same thermodynamic conditions (see Figure 10). We observe that the dormancy for most of the cryo-adsorbents is dominated by the adsorbed phase, and for compacted MOF-5 the dormancy is almost entirely determined by the properties of the adsorbed hydrogen phase. The order of highest dormancy follows the order of highest sorbent density (see Table 3) except for the $Cu_3(BTC)_2$ and CNS-201 materials that have low n_{max} values.

For this comparison at 100 bar maximal pressure and 80 K initial temperature, the dormancy of the CcH_2 system is less than half the lowest dormancy of the sorbent materials. If we allow a higher pressure vent limit of 208 bar for the CcH_2 tank (which benefits the approach as seen earlier), the dormancy increases to 50.5 Watt-days, the same as for compacted MOF-5 and MIL-101. Note that the various systems have different physical characteristics (total mass, different sorbent density, sorbent heat capacities, thicker wall for the high pressure CcH_2 system, etc.) that should be accounted for in a comprehensive comparison. These complexities will be discussed in the next section.

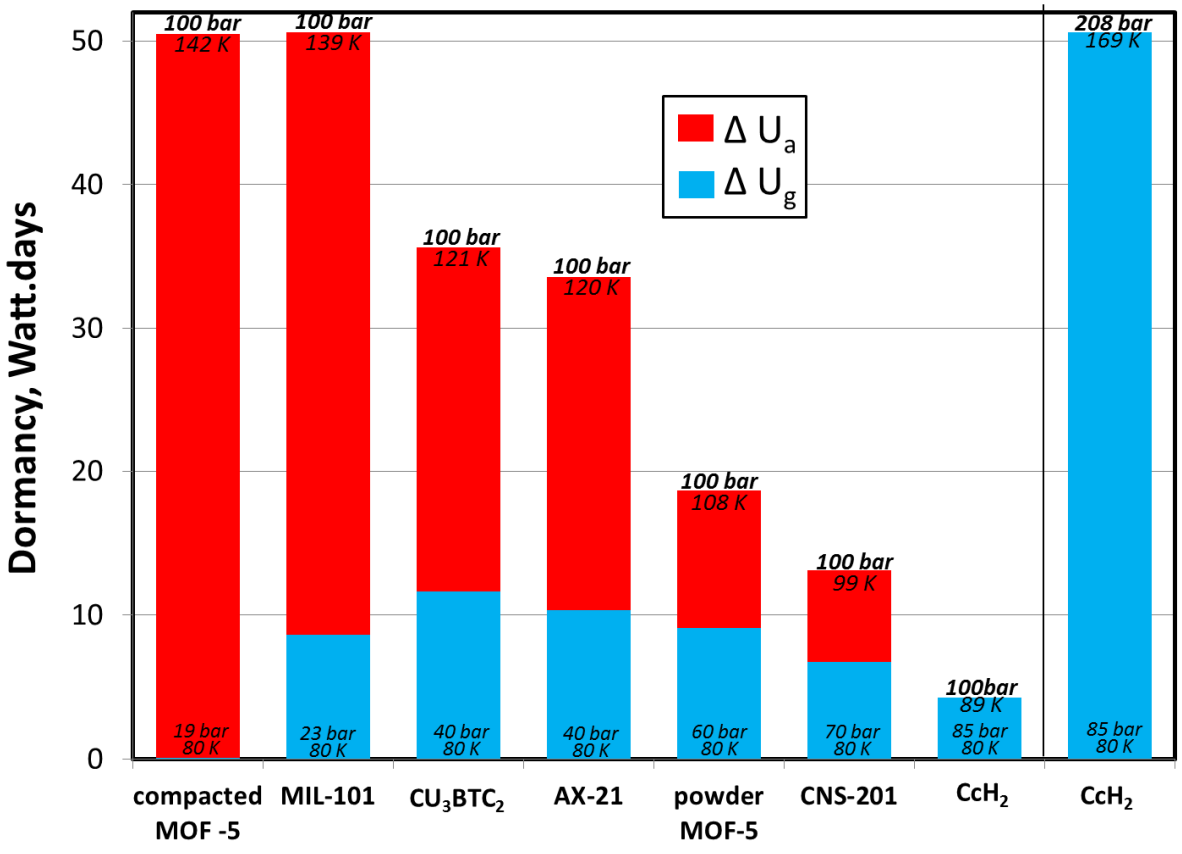

Figure 11. Dormancy comparison for 5 kgH_2 (total) initially at 80 K in a 190 L internal volume, 100 bar pressure vessel. The dormancy attributable to the adsorbed H_2 (ΔU_a) and not-adsorbed H_2 (ΔU_g) phases are shown. The pressure for the cryo-compression case that would equal the maximum dormancy cryo-adsorption material is also shown. The inner volume is completely filled with cryosorbent at its given density.

We describe the cryo-compressed and cryo-adsorption H_2 storage operational properties (e.g. system refueling, driving or parking) using a simple lumped parameter model, based on equations (4) and (5) below which represent the conservation of mass and energy, respectively [30] – see definitions of the terms in Table 1:

$$\frac{dm_{tot}}{dt} = \dot{m}_{in} - \dot{m}_{out} \quad (4)$$

$$\frac{dU_g}{dt} + m_s \frac{dU_a}{dt} + \frac{dU_s}{dt} + \frac{dU_{tank}}{dt} = h_{in}\dot{m}_{in} - h_{out}\dot{m}_{out} + Q \quad (5)$$

The mass conservation equation (4) can be stated in words as follows: any net change in the amount of hydrogen stored in the tank over time (by venting or fueling) must be accounted for by changes in the mass of hydrogen not adsorbed to the sorbent plus the mass of hydrogen adsorbed on the cryo-sorbent. The energy conservation equation (5) can be stated as follows: Using or fueling the tank changes the internal energy of the tank by virtue of the enthalpy of the hydrogen gas. The internal energy change of the tank is accounted for by the sum of the changes in the internal energies of the hydrogen that is not adsorbed, the hydrogen that is adsorbed, the sorbent itself and the surrounding tank structure.

One of the interesting intrinsic properties of a cryo-adsorption system is that the relative amounts of adsorbed and gaseous hydrogen can change with varying tank conditions. As a result, there is introduced an intrinsic dynamical complexity which our calculation describes. Figure 12 shows an example of single flow LH_2 fueling of a cryo-adsorption tank with powder MOF-5 material in a tank with 157 L internal volume. We assume that the tank was recently used in a vehicle for driving, and is being refilled starting with a residual 0.5 kg of H_2 in the tank at a residual 3 bar pressure (a typical shut-off pressure for a PEM fuel cell) and with an uniform material, H_2 and tank temperature of 86 K. The vessel is filled with constant entropy LH_2 until the pressure reaches the maximum value allowed by the tank wall thickness (here 350 bar), shown as dotted "fueling" lines. Subsequently, the tank is discharged at a constant flow rate (i.e. hydrogen consumption by the fuel cell) as shown by the "discharging" lines toward decreasing pressure. The discharge continues until the tank reaches the 3 bar minimum pressure for the fuel cell. The temperature variation of the MOF-5 + H_2 system is shown as the black lines in Figure 12.

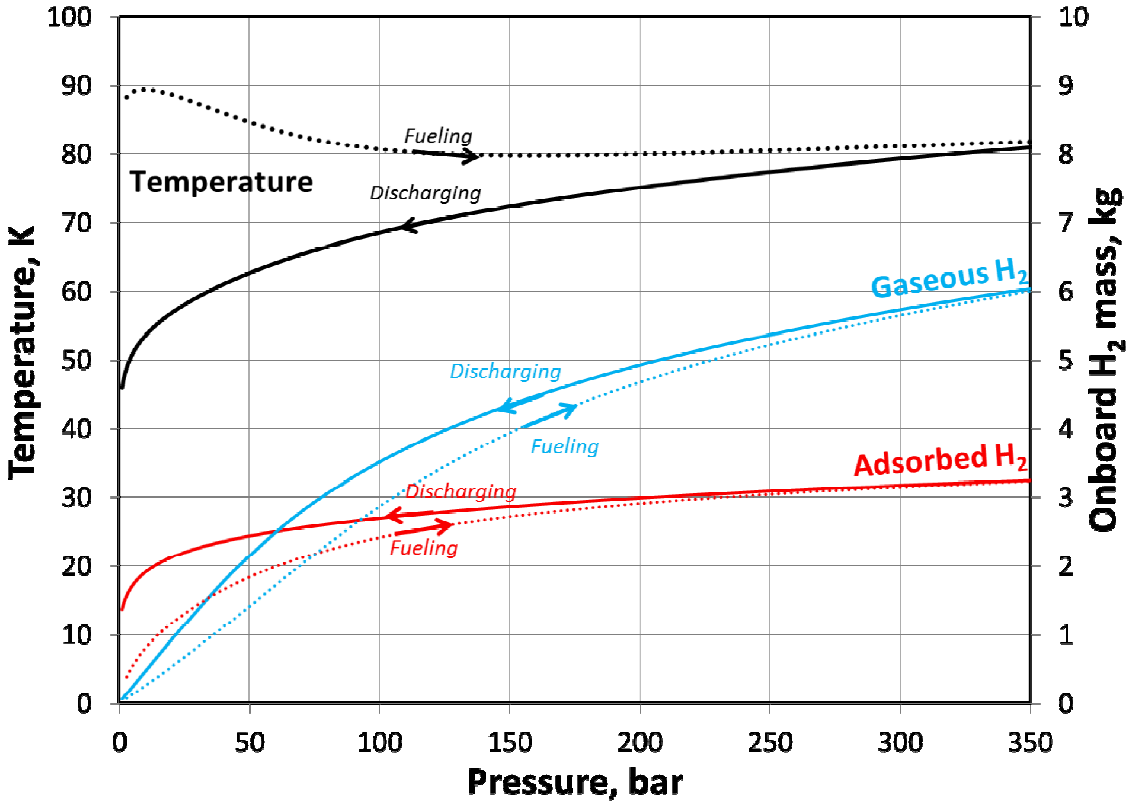

Figure 12. Onboard H_2 (adsorbed and gaseous) mass (blue and red lines, right axis) and temperature (black lines, left axis) for a powder MOF-5 system as a function of pressure during single flow LH_2 fueling – *increasing pressure dotted lines* (entropy = 4 kJ/kg/K, flow rate = 100 kg/hour) and during driving – *decreasing pressure continuous lines* (100 km/hour, 110 km/kg efficiency vehicle [4]), for a 156 L internal volume, 350 bar pressure vessel. We assume that the tank is being refilled starting with a residual 0.5 kg of H_2 in the tank at a residual 3 bar pressure, and with a uniform material, H_2 and tank temperature of 86 K

Several interesting phenomena are predicted in Figure 12. First, during fueling with cold (20 K) LH_2, the equilibrium temperature of the cryo-adsorbent material remains rather constant, as indicated by the black dotted line. Initially the temperature rises from 86 K to nearly 90 K. This temperature variation arises from the combined effects of a minor cooling associated with the enthalpy of vaporization of LH_2, and a larger heating effect arising from hydrogen pressurization and the exothermic nature of the adsorption process. With further fueling and pressure increases, the temperature drops to 80 K and remains relatively constant thereafter as 9.2 kg of hydrogen is loaded into the tank (6.0 kg as gaseous H_2, 3.2 kg as adsorbed H_2). The thermodynamics simulation of the discharge is very similar to single flow H_2 refueling, except the flow is much smaller, and exits the vessel at the specific enthalpy calculated from the conditions inside the tank. In order to simplify the explanation, we assume here that right after single flow refueling to 350 bar, the vehicle is driven at a constant speed of 100 km/hour with an efficiency of 110 km/kgH_2. We observe that while single flow refueling is at quasi constant temperature, driving

substantially cools the vessel from 80 to 47 K. This is due to the endothermic desorption and to the expansion of the gaseous H_2.

During fueling we see that although the adsorbed H_2 mass is larger than the gaseous H_2 mass at the beginning of the fill, the rate of adsorption reaches a maximum so that the gaseous H_2 mass is almost twice as large as the mass of adsorbed H_2 at the end of the fill (350 bar). During driving (discharge), the mass in the gas phase drops steadily, while the mass in the adsorbed phase reduces slowly. Once the pressure in the vessel reaches the minimum pressure of 3 bar, about 1.9 kg (total) of H_2 is still in the tank, mostly in the form of 1.5 kg of hydrogen adsorbed on the surface of powder MOF-5. This residual hydrogen corresponds to the "residual capacity" which requires external heat or pumping to extract.

These initial results (Figures 10 – 12) focused on the intrinsic properties of associated with the physical state of hydrogen in these two approaches, cold hydrogen fluid in the case of cryo-compressed storage, and a combined system of cold fluid and cold adsorbent in the case of the cryo-adsorption approach. In order to compare the two approaches in under more realistic conditions, we need to take full consideration of the storage system and its various components. The tank hardware can behave in a static way to affect gravimetric and volumetric density, but also in a dynamic way that affects the fueling capacities. We now present model results and predictions for the operational properties of cryo-compressed and cryo-adsorption systems in comparable, more realistic storage systems.

VI. Operational properties of cryo-compressed and cryo-adsorption hydrogen systems in comparable real tank systems

The performances of cryo-compression and cryo-adsorption hydrogen storage methods rely on the efficient use of pressure and sorbent material, respectively. Pressure and sorbent both improve volumetric density and dormancy, in exchange for extra mass and cost. How pressure and adsorption phenomena relate to each other in these two storage approaches for various operating conditions is very important to understand. Comparison between cryo-compressed and cryo-adsorption real tank systems are presented in this section.

1. Assumptions for the calculations

In order to understand the physical phenomena occurring in the cryo-compressed and cryo-adsorption systems, we examine by comparing two identical hydrogen vehicles whose storage system is based on either cryo-compression or cryo-adsorption. We assume the external volume associated with both approaches is fixed. The parameters of particular interests are: driving range (determined by onboard H_2 capacity and the mass of the storage system) and dormancy. Other criteria exist, see for example the targets established by the U.S. DOE [8, 18].

As shown in Figure 10, the cryo-adsorption and cryo-compressed approaches both preferably operate at cryogenic temperatures. Even if the optimal operational temperature might be different between the two approaches, it has been shown [10] that the heat transfer between the hydrogen and the environment does not vary significantly between 30 and 80 K when using Multi-Layer Vacuum Insulation (MLVSI). We therefore assume that the systems for both hydrogen storage methods use the same MLVSI insulation, with the same thickness, hence the same insulation volume and mass. No heat exchanger is considered, inside or outside the system (no extra volume, mass). Many different designs can be used and we choose not to discuss their engineering implementation here. Some designs can be found in [39], [40] . However, a (perfect) heat transfer has been considered for adsorption/desorption phenomena. Similarly, the LN_2 channel (which can take up to 19.24 kg and 16.42 L [33]) has been ignored. At last, the effect of a heating wire to access the residual density is not included in this study. As a result, all the components of both systems are assumed to be the same, except for the mass of the sorbent and the pressure vessel whose mass increases with pressure due to the need for thicker composite walls. We calculate relative difference in system mass: only the masses of the pressure vessel and the sorbent bed under different assumptions are given. It is assumed that cryogenic hydrogen is dispensed either from liquid H_2 (LH_2), using a cryogenic high-pressure pump [41], or using liquid nitrogen (LN_2), that would cool compressed hydrogen down to 80 K.

For simplicity, we also consider that all the H_2 in the tank is usable to power the car. Although this not a true statement (e.g. some H_2 might be used to power the electrical heater), this approximation was made in order to keep the variables of the comparison to a minimum.

Tamburello and co-workers [33] from the DOE Hydrogen Storage Engineering Center of Excellence recently presented real tank designs for cryo-adsorption. We consider those designs as a "baseline" design for our cryo-adsorption tank analysis: the pressure vessel is a Type I Aluminum (6061-T6) vessel, with a 0.38 m outer diameter and a rated pressure of 100 bar (wall thickness: 10.2 mm). This baseline cryo-adsorption pressure vessel has oblate sphere heads (the head height h is lower than inner radius R: $h = 2R/3$)**.** The overall system is similar to that depicted in Figure 8 for cryo-adsorption, in which the pressure vessel is surrounded by MLVSI and a secondary enclosure. The fueling method envisioned by the HSCoE is LN_2 cooling of the system (tank + H_2) at the fueling station, down to 80 K, which we consider our "baseline" refueling protocol. See Table 5 for the mass distribution of the different components of the "baseline" cryo-adsorption case.

Table 5. Mass distribution of the various components of the cryo-adsorption system designed by Tamburello et al [33].

Components	Mass, kg
Pressure vessel	62.45
LN_2 channel	19.24
Outer shell	15.35

Insulation	8.01
Boss, plug and support rings	1.28

715

716 Since the outer diameter and length of the cryo-adsorption and cryo-compression pressure
717 vessels are constrained to be equal and constant throughout the analysis, the effect of increasing
718 pressure is a decreasing inner volume (and diameter). Pressure vessels rated for pressures of
719 above 100 bar are considered here to be type III (composite overlapping a metallic liner), with an
720 Aluminum 6061-T6 liner with a 5 mm thickness [42]. An elastic analysis very similar to a
721 netting analysis [43] has been performed in order to compute the composite thickness as a
722 function of the maximum operating pressure, based on the method described in [44].
723 Assumptions for the calculations are summarized in Table 6, and the properties of the metallic
724 liner and the composite are shown in Table 7 and 8, respectively. The composite thickness is
725 assumed to be uniform around pressure vessel.

726 The elastic analysis takes into account initial loading and considers that the winding of the
727 composite is such that 3 layers of different orientation are used: 2 helical layers of equal
728 thickness (at -30 and +30 degrees) and 1 hoop layer (90 degrees), whose thickness is twice the
729 helical layer thickness. The total composite thickness is thus the sum of the thickness of those 3
730 layers. Figure 13 shows the variation of the total composite thickness as a function of the
731 maximum operating pressure based on an elastic analysis (more details can be found in [44]),
732 whose assumptions are described in Table 6. We observe that the thickness is a linear function of
733 the maximum operating pressure. Those results will be used in the rest of the analysis. Also, it is
734 assumed that the properties of the aluminum and the composite are constant with temperature.

735 **Table 6.** Assumptions for the elastic analysis performed to compute the composite thickness as a
736 function of pressure for a constant outer diameter pressure vessel (more details on the method
737 can be found in [44])

Liner	Al 6061-T6
Composite (fiber/epoxy)	T300/5208
Liner thickness	5 mm
Composite thickness	Varied with pressure
Outer tank diameter, m	0.38
Safety factor (ration between working and burst pressure)	2.25 ([45], [46])
ratio of the compressive stresses in the liner to those causing yielding on unloading	0.6
Helical winding angle	-30°, 30°
Number of layers	3 (-30°, 30°, 0°)
Ration between hoop and helical thickness	2
Ratio of strain in helical to hoop fiber	< 70%

738

739 **Table 7.** Properties of aluminum 6061-T6 (from [44], except density)

Modulus, GPa	68.9
Poisson coefficient	0.33
Yield stress, MPa	290
Shear modulus, GPa	26.5
Density, kg/m^3 [33]	2663

740

741 **Table 8.** Properties of carbon fiber T300 with 5208 epoxy (from [44], except density)
742

Axial modulus, GPa	153
Transverse modulus, GPa	11.2
Poisson coefficient for uniaxial stress and transverse strain	0.33
In-plane shear modulus, GPa	7.1
Fiber failure strain in tension	1.4 %
Fiber volume fraction	60 %
Density, kg/m^3 [46]	1580

743

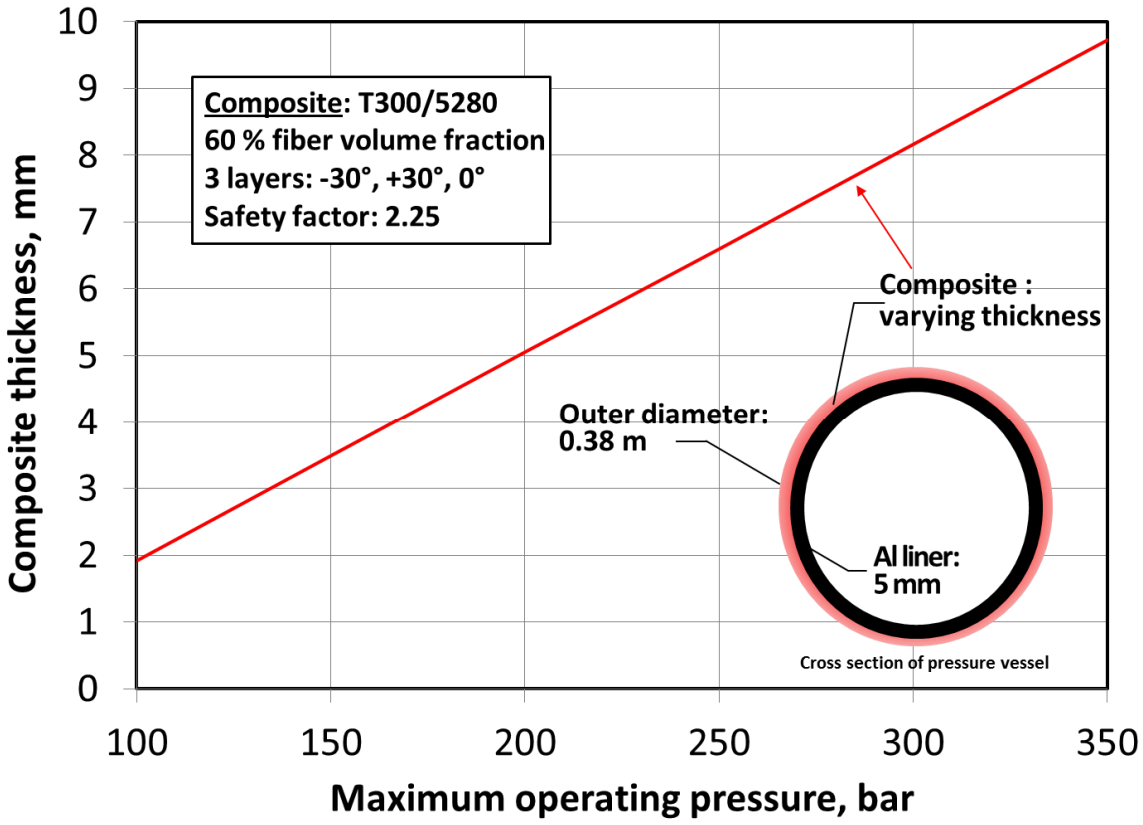

744

745 **Figure 13.** Variation of the composite thickness as a function of working operating pressure
746 using elastic analysis from [44] and based on the assumptions from Tables 6, 7 and 8. The outer

diameter is kept constant, so that the inner diameter (hence the inner volume) diminishes as the maximum operating pressure increases.

The inner volume calculation for the type III pressure vessels goes as follows. The inner pressure vessel volume enabling the storage of 6 kgH_2 at 100 bar and 80 K is first calculated (using Eq. 1) for each sorbent (powder MOF-5 or MIL 101). Assuming constant outer diameter (0.38 m) and 5 mm uniform Al liner thickness, the composite thickness required for 100 bar operation is calculated (see Figure 13). This determines the inner diameter. The inner length is calculated for each sorbent (taking into account the oblate sphere heads) to match the inner volume previously calculated. This step also enables to compute the outer length and diameter that will be held constant for any pressure. The last step consists in taking into account the effect of thicker wall at higher pressure using Figure 13. Table 9 summarizes the geometrical dimensions used for MOF-5 and MIL101.

Table 9. Internal volume, masses and outer dimensions of a pressure vessel that would hold 6 kgH_2 at 100 bar and 80 K, assuming oblate sphere heads (h=2R/3). The internal volume and mass of 350 bar operating pressure vessel that would fit in the same envelope are also given (last column).

	Internal volume @ 100 bar, L (Al/composite mass, kg)	**Outer diameter, m**	**Outer length, m**	**Outer volume, L**	**Internal volume @ 350 bar, L (Al/composite mass, kg)**
Powder MOF-5	169 (26.6 / 6.4)	0.38	1.721	185	156 (25 / 31)
MIL 101	136 (21 / 5)	0.38	1.385	147	124 (20 / 25)

Two refueling scenarios are considered here: LH_2 and 80 K refueling. In the first scenario, LH_2 is flowed at constant entropy directly into the tank using a LH_2 pump [41] and requires solving the mass and energy conservation equations (see Equations 4 and 5). In the second scenario (our baseline 80 K fill), we consider a system which has been pre-cooled to 80K, presumably using LN_2 cooling coils integrated to the tank architecture [33]. H_2 here is generally available as compressed at room temperature [47], and is either pre-cooled before entering the vessel or cooled directly inside the vessel. We consider that the equilibrium temperature of 80 K is reached given enough time and cooling and only equation (1) is used. About 30% of the energy content is typically required to remove the heat generated by the adsorption of hydrogen [30]. For both cryo-compression and cryo-adsorption storage, the initial tank condition chosen here is the minimum temperature for which the stored H_2 capacity is 0.5 kg [48], which correspond to the minimum delivery pressure of 3 bar [16].

2. Comparison between powder MOF-5 and cryo-compressed tanks

Let us consider first a 100 bar cryogenic tank with a 169 L internal volume. Various quantities of hydrogen can be stored in this tank depending whether a sorbent material (here: powder MOF-5) is present or not (CcH_2). This is analyzed in Figure 14, where the total amount of H_2 that can be stored in both systems as a function of temperature is reported. Note the residual capacity curves for the cryo-adsorption and CcH_2 approaches at 3 bar pressure. For powder MOF-5, the residual capacity is significant and rises steadily as the temperature decreases. This produces a clear identification of the refueling starting point (0.5 kg, 3 bar) at 90 K for the MOF-5 system. For the CcH_2 system, the residual capacity curve is smaller in overall magnitude, and varies less with temperature. As a result, there is a wider range of temperatures which yield capacities under 0.5 kg at 3 bar. For this reason and for comparison purposes with sorbent based systems, we consider LH_2 refueling from 60 K and 90K (and 0.5 kg) starting points for the CcH_2 system. Note however that the actual CcH_2 residual density is lower than 0.5 kg at those temperatures.

For 80 K baseline fueling (indicated by the black arrow), 6 kgH_2 can be stored inside the tank packed with 25.3 kg of powder MOF-5, while 5 kgH_2 can be stored in the absence of the sorbent material. This is due to the larger density of H_2 stored in the sorbent as opposed to the CcH_2 method at 100 bar pressure. Now let's consider LH_2 fueling. Starting with the powder MOF-5 material, the stored H_2 quantity is about the same as for 80 K filling. Note the almost vertical temperature profile in the LH_2 refueling of powder MOF-5 from 90 K (see also Figure 12). This flat thermal profile is due to the thermal mass of the sorbent material. As a result, due to this isothermal behavior, the 80 K fueling and the LH_2 fueling from 90 K produce the same 6 kg stored mass. In contrast, for the CcH_2 tank, we see that 8 kg of hydrogen can be stored by LH_2 refueling from the 90 K/0.5 kg initial state, and 9.8 kg can be stored by LH_2 refueling from the 60 K/0.5 kg residual capacity starting point for the CcH_2 system. The larger temperature decreases seen for CcH_2 (and the associated higher storage densities) can be attributed to the low internal energy of LH_2 that enables slower pressurization and thus more mass transfer. The two hydrogen storage systems vary in mass by 25.3 kg, i.e. the mass of the sorbent material. The pressure vessel alone weighs 33 kg.

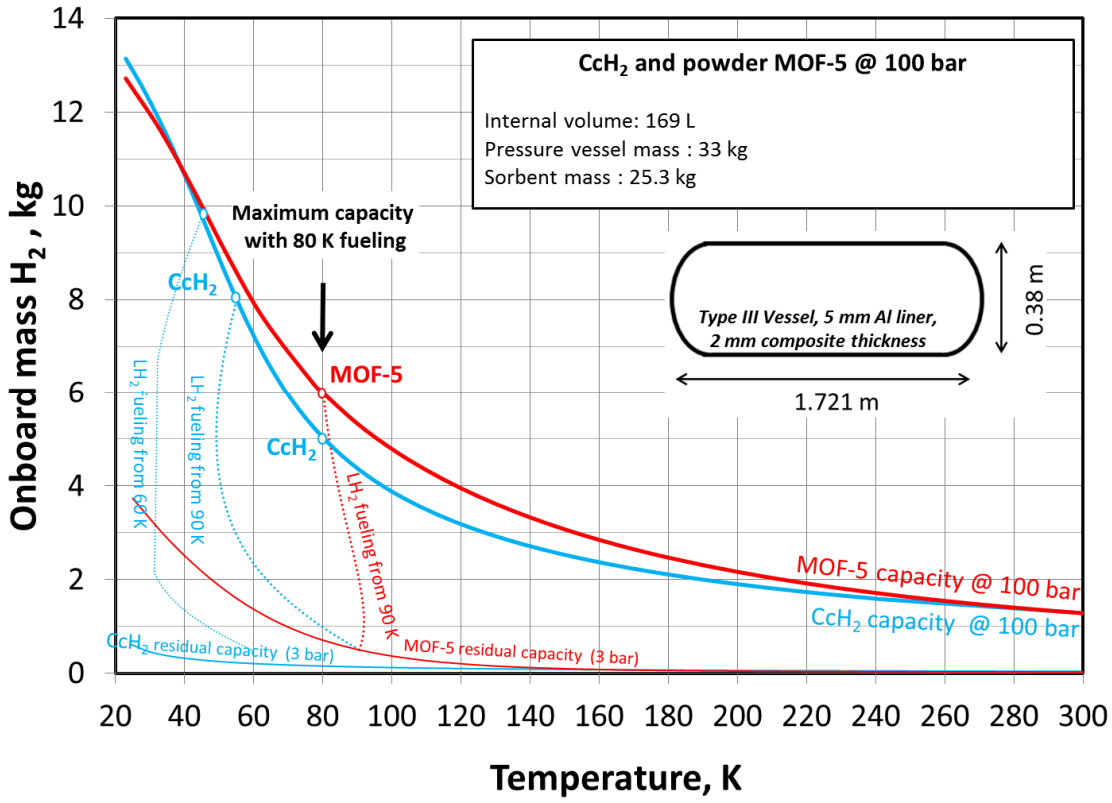

Figure 14. Amount of H_2 stored in 100 bar, 169 L internal volume cryogenics vessel as a function of temperature, whether powder MOF-5 is present or not. Both tanks have same external dimensions, as sketched on the figure, with an outer volume of 185 L (see Table 8). The downward pointing black arrow locates hydrogen capacities for the baseline 80K fill, as described in the text.

The influence of pressure is shown next in Figure 15, where the amount of H_2 stored in a 100 bar, 169 L vessel filled with powder MOF-5 is compared with the amount of H_2 stored in a 350 bar, 156 L CcH_2 system. The higher pressure CcH_2 system has a lower internal volume in order to account for thicker composite wall so that the total system volume (high-pressure vessel + insulation + secondary enclosure) is the same for the 100 bar cryo-adsorption and 350 bar CcH_2 systems.

More hydrogen can be filled in the CcH_2 system since higher densities can be reached at higher pressure: 9.5 kg assuming 80 K fueling and more than 11 kg using LH_2 fueling, versus 6 kg in the powder MOF-5 system at 80 K. The powder MOF-5 tank capacity cannot be increased further because 20 K LH_2 fueling does not reduce the sorption material temperature below 80 K due to the sorbent thermal mass.

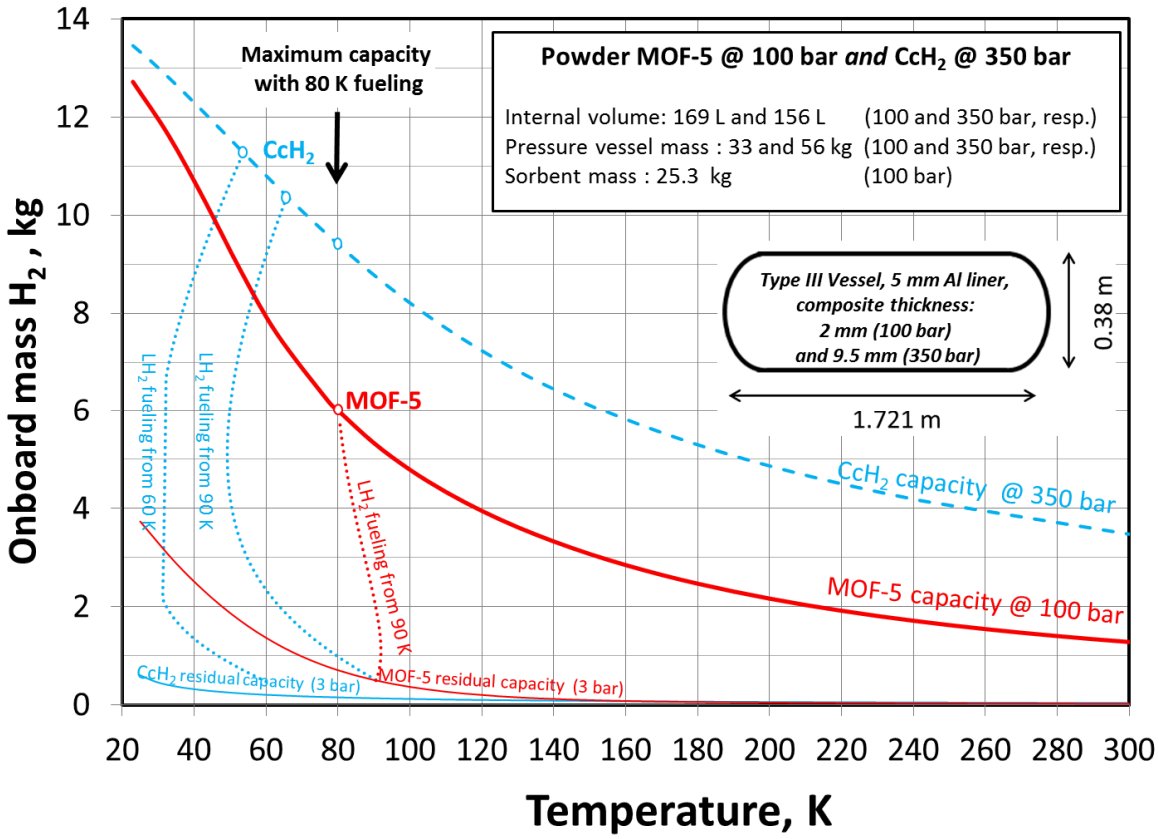

822

823 **Figure 15.** Amount of H_2 stored in 100 bar, 169 L powder MOF-5 system and a 350 bar, 156 L CcH_2
824 system as a function of temperature. For the 100 bar cryo-adsorption system, the tank internal volume is
825 169 L, the pressure vessel mass is 33 kg, and the powder MOF-5 mass is 25.3 kg. For the 350 bar CcH_2
826 tank, the internal volume is 156 L and the pressure vessel mass is 56 kg. Both vessels have the same
827 external dimensions, as sketched on the figure, with an outer volume of 185 L (see Table 8). The
828 downward pointing black arrow locates hydrogen capacities for the baseline 80K fill, as described in the
829 text.

830 Finally, we consider in Figure 16 a 350 bar cryogenic vessel filled with powder MOF-5. This
831 approach represents a "hybrid" approach, where both the effects of sorbents and pressure are
832 used to increase volumetric density and dormancy. Once more, the total system volume (high
833 pressure vessel + insulation) is considered to be held constant and equal to the systems showed
834 in Figures 14 and 15. Results for the CcH_2 system from Figure 14 are repeated in Figure 15,
835 along with results predicted for the 350 bar, 150 L internal volume vessel filled with powder
836 MOF-5. We observe that the H_2 capacity lines for powder MOF-5 and CcH_2 are close to each
837 other, with the powder MOF-5 system providing larger capacities at temperatures warmer than
838 80 K. The extra storage afforded by the adsorbed hydrogen phase of the sorbent material is
839 almost cancelled out by the space needed by the material itself in the vessel which excludes
840 space for storage of high-pressure gas. In other words, under these high pressure conditions,
841 powder MOF-5 plays a small (~10%) net positive role in increasing the stored hydrogen mass

over the case where no material is present for temperatures greater than ~100 K. For temperatures below ~ 80 K, the presence of the cryo-adsorbent material becomes punitive. The maximal H_2 capacities for powder MOF-5 are 9.3 kg independent of fueling (80 K or LH_2), and are actually equal to the maximum CcH_2 capacity assuming 80 K fueling, but are 10.3 to 11.3 kg for the CcH_2 system filled with LH_2, depending on the initial temperature (90 K or 60 K, respectively) of the starting CcH_2 tank with 0.5 kg. Note that the hybrid system (with sorbent) is 23.4 kg heavier than the CcH_2 tank due to the mass of the powder MOF-5 material.

It is interesting to see the temperature variations of the two systems in Figure 16 during the different fills. For the LH_2 fueling from 90 K/0.5 kg, the cryo-adsorption system is nearly isothermal as discussed above. However, large temperature variations are seen for the CcH_2 system. For refueling to 350 bar pressure from the 60 K/0.5 kg starting point on the CcH_2 residual capacity curve, the hydrogen temperature drops to ~30 K, and then increases in temperature nearly all the way back to 60 K at 350 bar due to compression heating. The constant temperature (~30 K) part of the fill corresponds to fueling through the 2-phases part of the phase diagram.

The main results for the influence of pressure and powder MOF-5 on the H_2 storage capacity and the mass of the system are summarized in Figure 17.

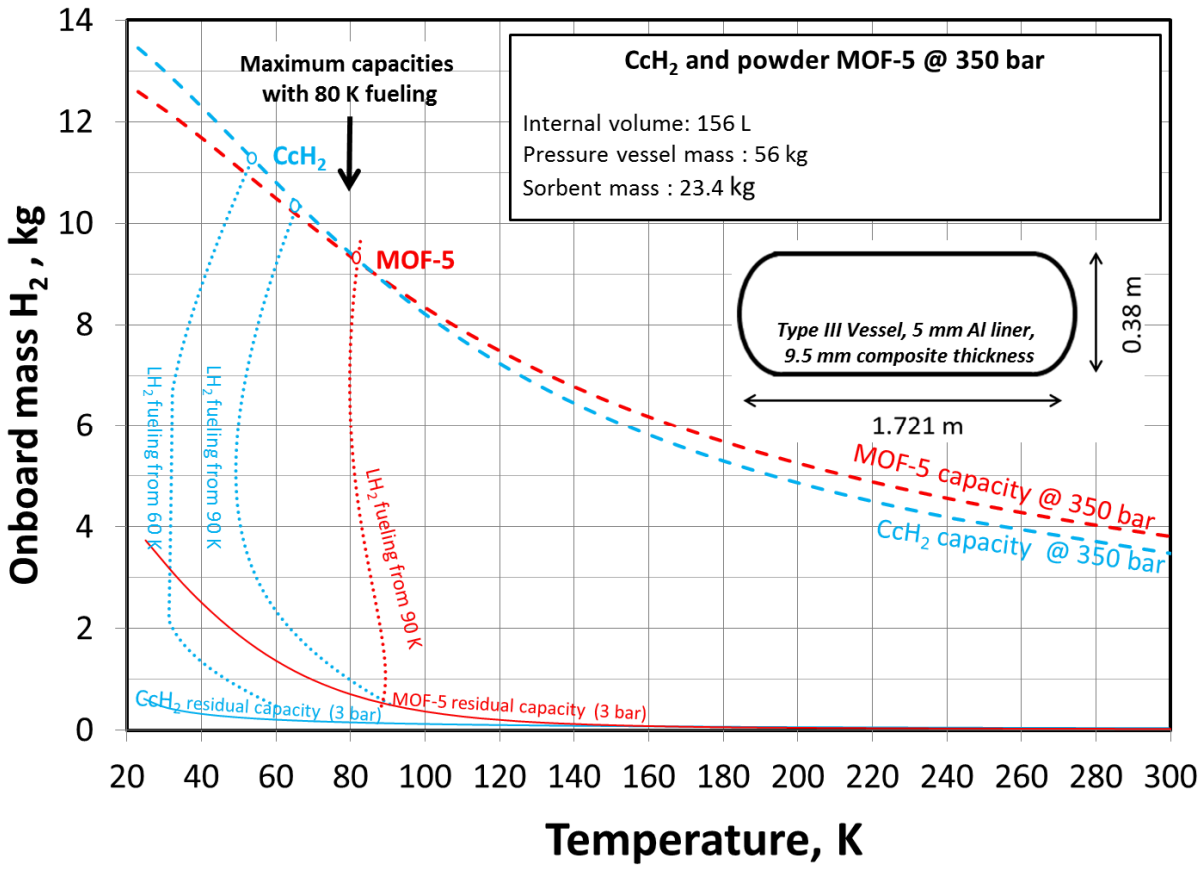

Figure 16. Maximum H_2 capacities stored in 350 bar, 156 L internal volume cryogenic vessel versus temperature, as a function of the presence or absence of MOF-5 for the 2 fueling methods. Both vessels have the same external dimensions, as sketched on the figure, with an outer volume of 185 L (see Table 8). The downward pointing black arrow locates hydrogen capacities for the baseline 80K fill, as described in the text.

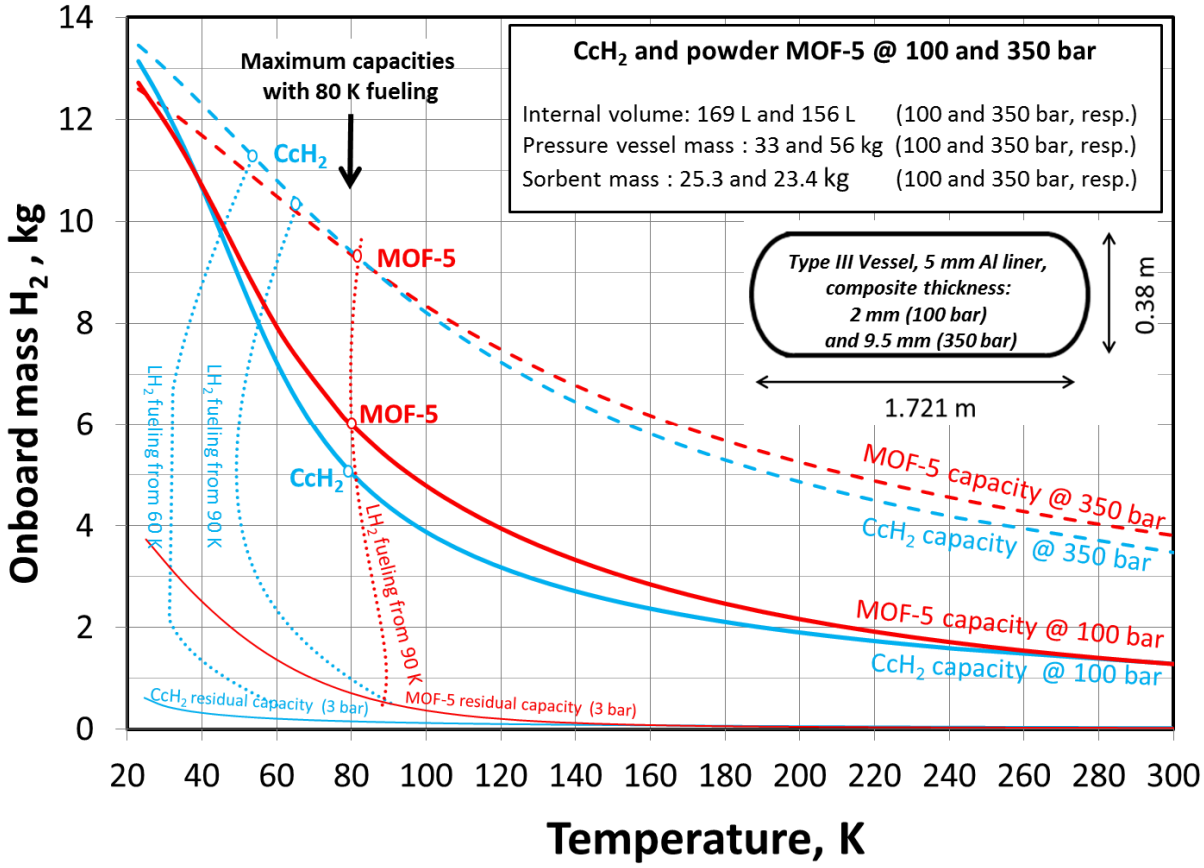

Figure 17. Summary of the influence of pressure and powder MOF-5, as well as fueling method, on the onboard stored H_2 and mass of pressure vessel. All vessels have the same external dimensions, as sketched on the figure, with an outer volume of 185 L (see Table 8). The downward pointing black arrow locates hydrogen capacities for the baseline 80K fill, as described in the text.

As shown in Figure 11 at 100 bar pressure, the use of adsorption material increases dormancy, since the adsorbed phase can absorb energy (second term in Eq. (4)), and thus increases the energy needed to reach the vessel operating pressure limit. Dormancy depends on the fill level of the vessel, the initial temperature and also the final conditions (i.e. operating pressure). In order to study the influence of the pressure and the use of adsorption material on dormancy, we consider 2 cases. First we examine the same amount of H_2 (5 kg) initially stored at 80 K with varying operating pressure limit (i.e. vent pressure) as shown in Figure 18. Second, we use a fixed dormancy (50 Watt-days, corresponding to 10 days of parking assuming a 5 Watts heat transfer rate) and examine how much H_2 can be stored given that design dormancy criterion, i.e.

the range of the vehicle, for various total system masses (pressure vessel + sorbent + H_2), with H_2 initially stored at 80 K, as shown in Figure 19. Once again, all the systems that are studied occupy the same total volume.

In Figure 18, the different dormancies for the MOF-5 and CcH_2 systems each storing 5 kg of H_2 at a given maximum operating pressure are connected by black lines, with the pressure rating indicated. The powder MOF-5 systems are heavier than CcH_2 systems for any pressure limit. We observe that for a given venting pressure limit, the powder MOF-5 system has a greater dormancy than the CcH_2 system. As the pressure limit increases, the dormancy for both systems increase and the mass of the storage vessels increase. However, the dormancy benefit of having the adsorption material present grows with increasing pressure. A 350 bar powder MOF-5 system has a dormancy of 220 Watt-days for 5 kgH_2 initially stored at 80 K while a 350 bar CcH_2 system has a dormancy of 160 Watt-days under the same conditions, although the CcH_2 system is ~ 25 kg lighter. Also shown in Figure 18 is the variation of pressure vessel mass yielding a given dormancy for the CcH_2 system initially starting at 5 kg of H_2 at 50 K temperature and 45 bar pressure. For a given pressure vessel mass (fixed maximum operating pressure), the dormancy is higher for the 50 K/45 bar curve because the system starts at a lower pressure and temperature. Thus it takes longer to get to the vent pressure limit (i.e. dormancy is increased). A 100-bar pressure-limit powder MOF-5 system weighs about ~5 kg more than a 350-bar maximum operating pressure CcH_2 system.

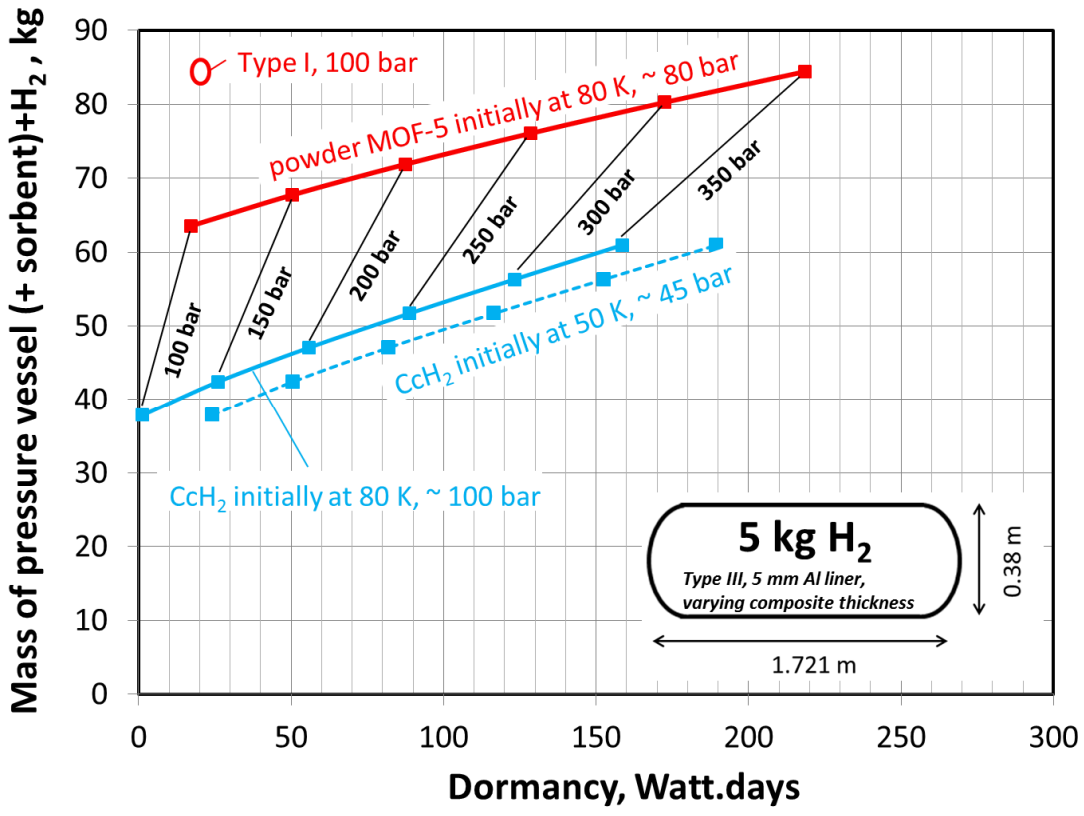

Figure 18. Mass of pressure vessel + sorbent +H_2 vs. dormancy for the CcH_2 and the powder MOF-5 systems filled with 5 kg H_2 initially at 80 K. The performance of a Type 1 (Aluminum), 100 bar, powder MOF-5 system is also reported for comparison. The different dormancies for the powder MOF-5 and CcH_2 systems each storing 5 kg of H_2 at a given maximum operating pressure (100 to 350 bar) are connected by black lines, with the pressure limit indicated. All vessels have the same external dimensions, as sketched on the figure, with an outer volume of 185 L (see Table 8).

The mass difference between the two approaches can be argued to be of second order compared to the total weight of a vehicle. However, the large gravimetric heating value of H_2 makes the payload critical: an extra kg of H_2 could mean an extra 100 km of range [4]. This is examined in Figure 19, where it is considered that a dormancy of 50 Watt-days is a fair design criterion, as it corresponds to a 5 Watts storage system heat leak that would be parked for 10 days without venting, a typical airport parking scenario. A calculation similar to Figure 18 was done, except that the dormancy was fixed to 50 Watt-days and the maximum onboard capacity (assuming 80 K fueling) was varied. We report on Figure 19 the maximum H_2 capacity as a function of total mass (including pressure vessel, sorbent material and H_2). For a total mass of 60 kg and a fixed 50 Watt-days dormancy, either 3.5 kgH_2 can be stored in a 100 bar powder MOF-5 system or 7 kgH_2 in a 250 bar CcH_2 system, a factor 2 in range. A 50 K initial temperature fill would triple the range of a 60 kg total mass design.

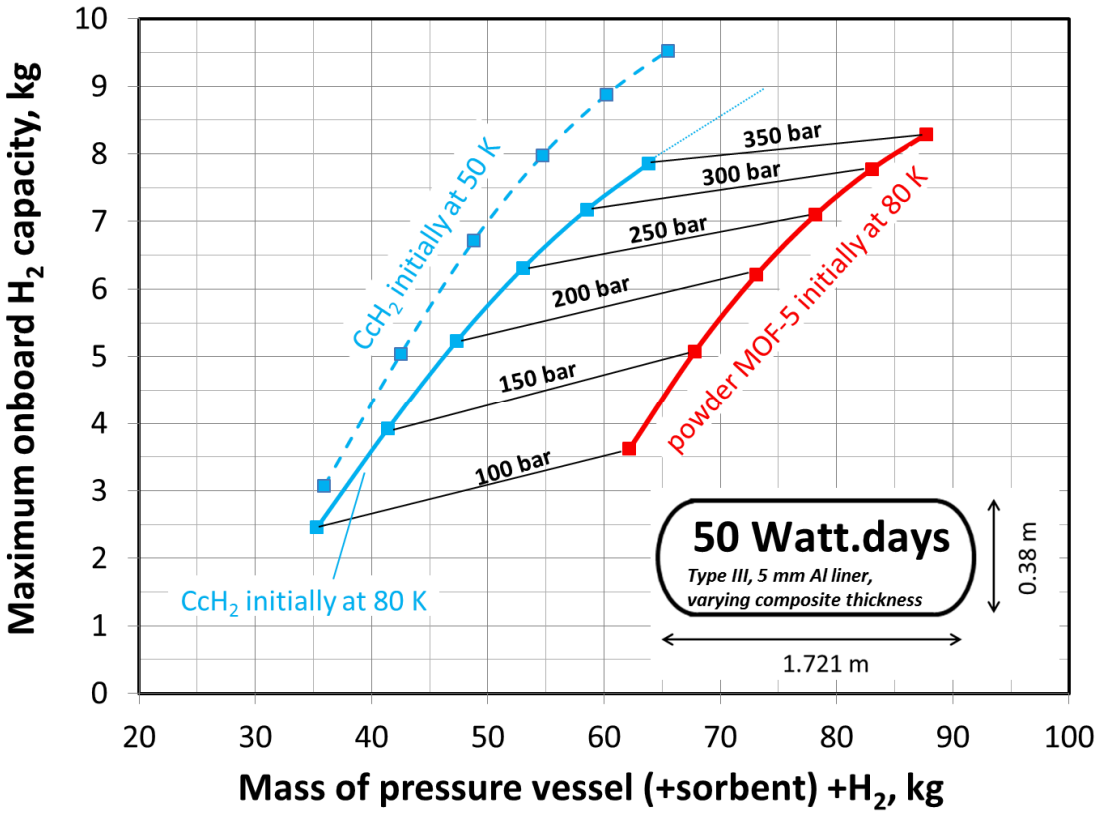

Figure 19. Onboard H_2 capacity as a function of the total mass of the system (pressure vessel + sorbent + H_2) for pressure vessels whose maximum operating pressure varies between 100 and 350 bar, assuming a 50 Watt-days engineering design. All vessels have the same external dimensions, as sketched on the figure, with an outer volume of 185 L (see Table 8).

3. Comparison between MIL-101 and cryo-compressed tanks

From Figure 10, we see that MIL-101 exhibits highest hydrogen storage densities across the whole range of pressure when compared to the other sorbent materials. A similar set of analyses as reported in the previous section for powdered MOF-5 is now conducted for MIL-101. The capacity comparisons are reported in Figure 20. The total volume (147L, see Table 8) is such that 6 kgH_2 can be stored at 80 K and 100 bar using MIL-101. The first thing to notice is that the internal volumes for MIL-101 are smaller than for powder MOF-5. This finding is consistent with the higher overall hydrogen storage density of MIL-101. Secondly, the MIL-101 sorbent mass is almost twice as large as that reported in Figure 17 for powder MOF-5 because of the relatively high sorbent density of the MIL-101 material (see $\rho_{sorbent}$ in Table 3). A third point of interest is that for MIL-101, when the tank needs to be refilled at 3 bar and 0.5 kg of H_2, the temperature of the MIL-101 cryo-adsorbent is a relatively high 120 K (see Figure 20). Using LH_2 to refill the MIL-101 tank from this point is nearly isothermal, as was seen for powder MOF-5 (Figs. 12 and 17). Refueling from the 120 K/3 bar point on the MIL-101 residual capacity curve leads to stored hydrogen masses of 4.4 kg at 100 bar and 6.5 kg at 350 bar maximal pressures, respectively.

At 100 bar, MIL-101 enables higher storage capacity (6kg) with the baseline 80 K fill (indicated by the black arrow) than the same fill of CcH_2 (4 kg). LH_2 fueling of the 100 bar CcH_2 system fills the tank to a mass of 6.8 – 7.5 kgH_2 (see blue dotted lines: LH_2 fueling from 60 and 80 K). For 80 K refueling to a 350 bar pressure limit, Figure 19 shows the onboard mass of H_2 is almost the same between CcH_2 and MIL-101. Comparing the storage density of MIL-101 at 100 bar to that of CcH_2 at 350 bar, we see the CcH_2 storage capacity is 2.5 to 3 kgH_2 larger. For a given pressure rating, the mass of the sorbent tank is higher than the mass of the CcH_2 tank by an amount equal to the mass of the sorbent.

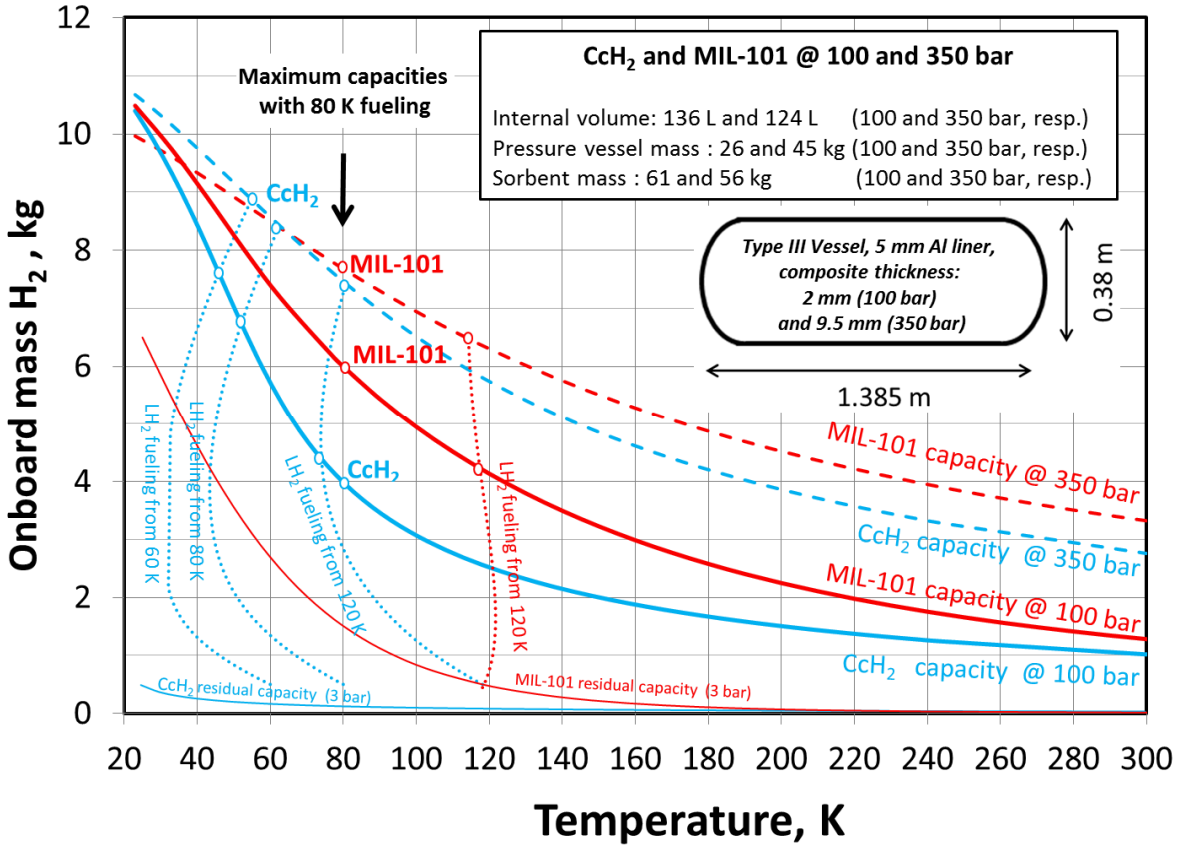

Figure 20. Comparison of the maximum onboard H_2 capacities between CcH_2 and MIL-101 versus temperature, for 2 pressures (100 and 350 bar) and the 2 fueling methods. The total volume (147 L, see Table 8) is the same for all systems. The internal volume of the pressure vessel is 136 L and 124L for 100 bar and 350 bar pressure ratings, respectively. The pressure vessel mass is 26 kg and 45 kg for the 100 bar and 350 bar tanks, respectively. The MIL-101 sorbent mass is 61 kg and 56 kg for the 100 bar system and the 350 bar system. Note that the MIL-101 sorbent mass scales with the internal volume for the two pressure ratings.

In analogy with Figure 18 for powder MOF-5, dormancy comparisons between MIL-101 and CcH_2 are shown in Figure 21. Two dormancy analyses are performed. One analysis is for a fixed 5 kg hydrogen mass initially at 80 K, with variation in the vessel maximum vent pressure (Figure 21). A second dormancy analysis is shown for an equal system mass with varying stored hydrogen mass (Figure 22). Although the results are qualitatively similar to the prior results for powder MOF-5, there are some noteworthy differences. First, we see that for a given dormancy, the mass of the pressure vessel + sorbent is higher for MIL-101 than powder MOF-5. This is explained by the higher material density of the MIL-101 sorbent. Second, based on Figure 21, the high MIL-101 sorbent density enables larger dormancy than for CcH_2. At 350 bar, the dormancy of the MIL-101 system initially storing 5 kgH_2 at 80 K is 225 Watt-days. In comparison at 350 bar, the CcH_2 system under the same conditions has a dormancy of 80 Watt-days.

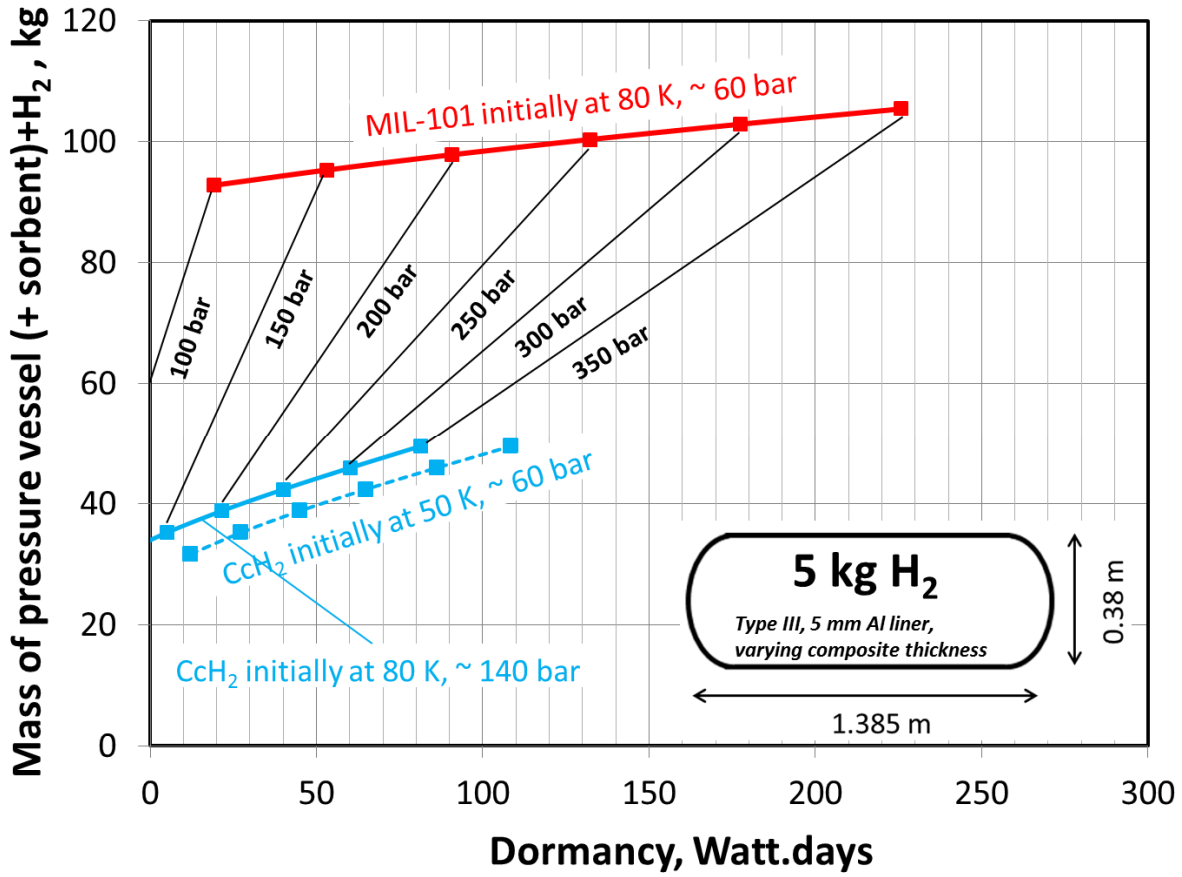

966

967 **Figure 21.** Mass of pressure vessel + sorbent and pressure vs. dormancy for the CcH_2 and the MIL-101
968 systems filled with 5 kg H_2 initially at 80 K. The performance of a Type 1, 100 bar, MIL-101 system is
969 also reported for comparison. All vessels have the same external dimensions, as sketched on the figure,
970 with an outer volume of 147 L (see Table 8).

971 Dormancy comparisons using fixed system mass but varying amount of stored H_2 are shown in
972 Figure 22. Here, both systems weigh 88 kg, but are filled with different amount of H_2 at initially
973 at 80 K. Larger amount of H_2 can be stored in the CcH_2 system because of the higher pressure
974 and the amount can be stored over a longer time (larger dormancy). Also shown in Figure 22 is
975 the dormancy for a 44 kg 350 bar CcH_2 vessel, with higher dormancy than a 100 bar MIL-101
976 100 bar system, for a mass 44 kg less.

977

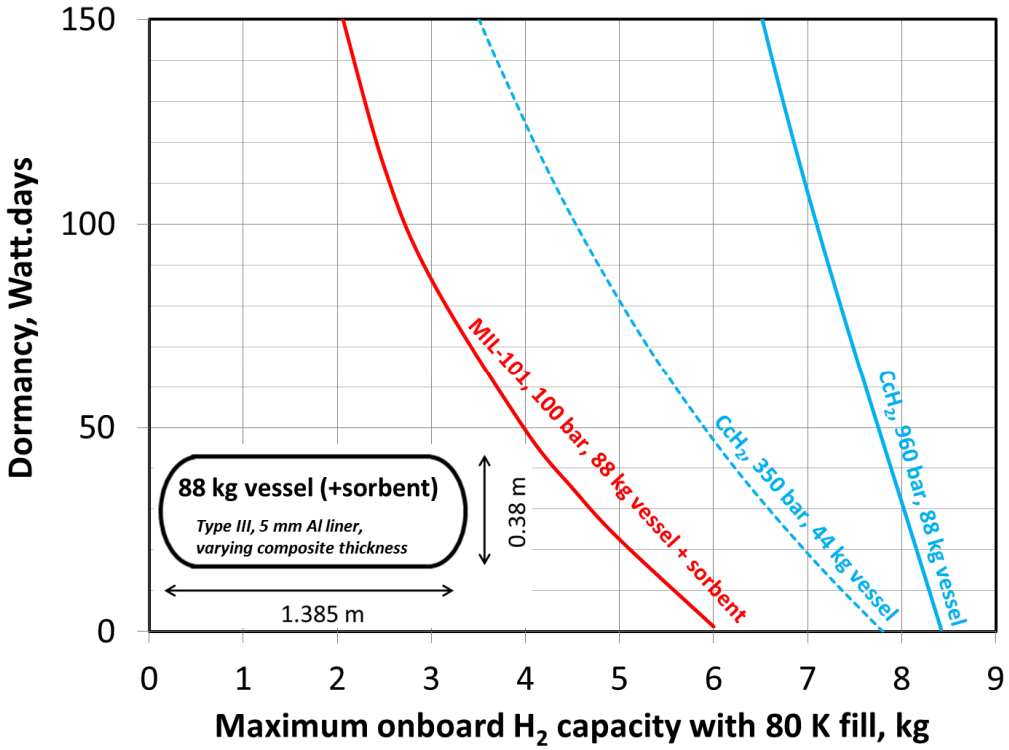

978

979 **Figure 22.** Dormancy as a function of the amount of H_2 initially at 80 K for 88 kg systems: CcH_2 at 960
980 bar and MIL-101 at 100 bar. For comparison, the dormancy of a 350 bar CcH2 vessel weighing 44 kg is
981 shown. (see text and Figure 21 for more explanation). All vessels have the same external dimensions, as
982 sketched on the figure, with an outer volume of l47 L (see Table 8).

983

984 # VII. Summary and Conclusions

985 A comparative analysis of cryo-compression and cryo-adsorption storage approaches was
986 presented based on a lumped parameter thermodynamic model, with the overall scope of
987 elucidating the role of pressure and sorbent materials in increasing on-board hydrogen capacity
988 and dormancy for cryogenic applications. . The assumptions made for that analysis are critical to
989 the outcome results and we invite the reader to review them at the beginning of Section VI). The
990 thermodynamics properties of H_2 combined with those of the sorbent play central roles in
991 determining on-board hydrogen capacity, dormancy, tank volume and weight, refueling capacity
992 and the dynamics of the tank temperature during refueling. These phenomena are described by
993 developing appropriate equation of state, and mass and energy balance equations for hydrogen in
994 the presence or absence of cryo-adsorbent for static systems and during refueling. The main
995 differences in the behavior of the two storage systems stem from how adsorption affects stored
996 hydrogen density, how the quantity of the absorbed phased changes with temperature and
997 pressure (which affects fill capacity and dormancy), and the dynamic thermal behavior of the
998 adsorbed hydrogen during charging (which produces heat) and discharging (which cools the

adsorbent). These phenomena are described for a variety of candidate sorbent materials, with a focus on MOF-5 and MIL-101 as the most promising of the sorbent materials discovered to date. The calculations were performed for the CcH_2 and cryo-adsorption tanks occupying the same volume in a vehicle, to allow a more straightforward comparison.

The optimal operating pressure regimes for each approach were identified. For cryo-compressed storage, the most advantageous pressure is as high as can be tolerated (but ~ 350 bar and above) and for as low a temperature as can be reached, typically below 77 K. For cryo-adsorption, the most optimal conditions for high density hydrogen storage are ~ 100 bar and temperatures below 77K.

The behavior of a cryo-adsorption storage system during filling with a liquid hydrogen pump is qualitatively different from CcH_2 filling. Thermodynamic investigation of single flow LH_2 fueling of cryo-adsorption MOF-5 and MIL 101 vessels at cryogenic temperatures were showed to be was almost isothermal (temperature at the beginning of the fill at 0.5 kg H_2 is very similar to the final temperature at the maximum rated pressure). This behavior is due to the combined effects of the enthalpy of vaporization of LH_2, the exothermic nature of the adsorption process, the thermal inertia of the sorbent thermal mass and the heating of pressurization. During LH_2 refueling, the CcH_2 tank temperature changes more as a result oflower thermal inertia .

Comparative analyses of operational properties (temperature and H_2 content variations with refueling using either single flow pressurized LH_2 or 80 K fueling (LN_2 temperature)) were conducted for the MOF-5 and MIL-101 cryo-adsorption tanks and CcH_2 tank at 100 bar pressure, for the CcH_2 system at 350 bar, and for a hybrid system in which sorbent is included in the high pressure tank. The analyses allow an assessment of stored hydrogen capacities and system weight for the two storage approaches for a variety of conditions of pressure, temperature and refueling strategies. The hybrid tank operating at high-pressure with cryo-sorbent inside increases storage beyond that of CcH_2 alone by 10% (sorbent = MOF 5) or 20% (sorbent = MIL101) at temperatures down to 80 K, when the hybrid tank and the CcH_2 have the same capacity. For temperatures below 80 K, having the sorbent material brings a density penalty, since the skeletal structure excludes cold gas at 350 bar pressure. Similarly as the pressure increases, the density of hydrogen in the adsorbed phase saturates whereas the density of compressed hydrogen continues to increase with pressure, eventually overtaking the adsorbed density at the breakeven pressure, beyond which the density of compressed hydrogen remains larger. This breakeven pressure strongly depends on temperature. At large enough pressures, the presence of the adsorbent will become detrimental and any gain in density will be offset by the loss in volume due to the skeletal volume of the adsorbent in the tank.

The dependence of system dormancy on maximum rated pressure, stored hydrogen mass, and the initial fueling conditions was comprehensively examined for MOF-5 and MIL-101 and compared with CcH_2 under similar conditions, once again assuming identical outer volume. For the same pressure rating of a storage system, the adsorption process will generally lead to

improved dormancy due to the endothermic nature of the desorption process, at the expense of added system weight. Our calculations showed that the dormancy increase is largely due to enthalpy of desorption for the adsorbed phase, rather than the contribution from hydrogen in the non-adsorbed phase, or thermal contributions from the sorbent skeletal mass itself.

In conducting this comparative analysis of the cryo-compression and cryo-adsorption hydrogen storage methods, we have intentionally not tried to assess which one is "better" or tried to choose a "winning" approach. Such a selection is not generally possible, since the choice of any hydrogen storage technology would depend very much on the end application, and even within a class of end applications, circumstances unrelated to the chemistry and physics of these approaches may be determinate. For example, the added mass that typically accompanies the cryo-adsorption method may be viewed negatively in some weight-sensitive applications, but a minor consideration for other applications. Likewise, the higher pressures that typically accompany the cryo-compressed technique could be viewed negatively in applications with high-pressure safety concerns, but viewed as a technically solved problem by other end users with different requirements. The cryogenic temperature needed for both techniques could be viewed as problematic for application situations without access to liquid hydrogen or liquid nitrogen (for 80 K fueling), or as a complete "non-issue" for those scenarios with developed LH_2 or LN_2 infrastructure. Our objective here has been to investigate the thermodynamic and chemical phenomena occurring when cold hydrogen is introduced into a storage tank with or without a cryo-adsorption material present, how adding cold hydrogen to these storage systems affects the quantity of hydrogen stored, the dormancy of the stored hydrogen tank system, how pressure affects capacity and dormancy, and the system masses and volumes (inner and outer) associated with the different scenarios. By performing a comparative analysis, we hope we have clarified the science of each approach individually, identified the regimes where the attributes of each can be maximized, elucidated the properties of these systems during refueling, and probed the possible benefits of a combined "hybrid" system with both cryo-adsorption and cryo-compression phenomena operating at the same time.

Acknowledgements

The authors of this work are from three different institutions. It was partially performed under the auspices of the U.S. Department of Energy by Lawrence Livermore National Laboratory under Contract DE-AC52-07NA27344. This project was partially funded by DOE, Office of Fuel Cell Technologies, Ned Stetson and Erika Sutherland, Technology Development Managers. Sandia National Laboratories is a multi-program laboratory managed and operated by Sandia Corporation, a wholly owned subsidiary of Lockheed Martin Corporation, for the U.S. Department of Energy's National Nuclear Security Administration under contract DE-AC04-94AL85000. This work was also funded by the Natural Science and Engineering Research Council's (NSERC) H2Can Strategic Network and benefited from the NSERC Strategic Network Enhancement Initiative program.

References

[1] Keller JO, Gillie S, Schoenung S, Klebanoff LE. The Need for Hydrogen-based Energy Technologies in the 21st Century. Hydrogen Storage Technology, Materials and Applications, Boca Raton: Taylor & Francis; 2012, p. 3.

[2] Klebanoff LE, Keller JO, Fronk M, Scott P. Hydrogen Conversion Technologies and Automotive Applications. Hydrogen Storage Technology, Materials and Applications, Boca Raton: Taylor & Francis; 2012, p. 31.

[3] Wallner T, Lohse-Busch H, Gurski S, Duoba M, Thiel W, Martin D, et al. Fuel economy and emissions evaluation of BMW Hydrogen 7 Mono-Fuel demonstration vehicles. International Journal of Hydrogen Energy 2008;33:7607–18.

[4] Paster MD, Ahluwalia RK, Berry G, Elgowainy A, Lasher S, McKenney K, et al. Hydrogen storage technology options for fuel cell vehicles: Well-to-wheel costs, energy efficiencies, and greenhouse gas emissions. International Journal of Hydrogen Energy 2011;36:14534–51.

[5] Toyota unveils own high-pressure H2 tanks for FCVs. Fuel Cells Bulletin 2005;2005:1.

[6] Bowman B, Klebanoff LE. Historical Perspectives on Hydrogen, its Storage and Applications. Hydrogen Storage Technology, Materials and Applications, Boca Raton: Taylor & Francis; 2012, p. 65.

[7] Gardiner M. Energy requirements for hydrogen gas compression and liquefaction as related to vehicle storage needs 2009.

[8] Klebanoff LE. Editor's Epilogue and Acknowledgements. Hydrogen Storage Technology, Materials and Applications, Boca Raton: Taylor & Francis; 2012, p. 427.

[9] California Environmental Protection Agency Air Ressources Board. Staff report: Initial statement of reasons, Advanced Clean Cars, 2012 Proposed Amendments To The Clean Fuels Outlet Regulation. 2011.

[10] Aceves SM, Petitpas G, Espinosa-Loza F, Matthews MJ, Ledesma-Orozco E. Safe, long range, inexpensive and rapidly refuelable hydrogen vehicles with cryogenic pressure vessels. International Journal of Hydrogen Energy 2013;38:2480–9.

[11] Ahn C, Purewal J. Storage Materials Based on Hydrogen Physisorption. Hydrogen Storage Technology, Materials and Applications, Boca Raton: Taylor & Francis; 2012, p. 213.

[12] Johnson T, Bénard P. Solid-State H2 Storage System Engineering: Direct H2 Refueling. Hydrogen Storage Technology, Materials and Applications, Boca Raton: Taylor & Francis; 2012, p. 347.

[13] Bowman B, Anton D, Stetson N. Engineering Assessments of Condensed-Phase Hydrogen Storage Systems. Hydrogen Storage Technology, Materials and Applications, Boca Raton: Taylor & Francis; 2012, p. 385.

[14] Ahluwalia RK, Hua TQ, Peng JK. On-board and Off-board performance of hydrogen storage options for light-duty vehicles. International Journal of Hydrogen Energy 2012;37:2891–910.

[15] Ahluwalia RK, Hua TQ, Peng J-K, Lasher S, McKenney K, Sinha J, et al. Technical assessment of cryo-compressed hydrogen storage tank systems for automotive applications. International Journal of Hydrogen Energy 2010;35:4171–84.

[16] http://www1.eere.energy.gov/hydrogenandfuelcells/storage/pdfs/targets_onboard_hydro_storage.pdf, accessed Nov. 20, 2012 n.d.

[17] Petitpas G, Aceves SM. Modeling of sudden hydrogen expansion from cryogenic pressure vessel failure. International Journal of Hydrogen Energy 2013;38:8190–8.

[18] Klell M. Storage of Hydrogen in the Pure Form. In: Hirscher M, editor. Handbook of Hydrogen Storage, Wiley-VCH Verlag GmbH & Co. KGaA; 2010, p. 1–37.

[19] Peschka W, Wilhelm EA, Wilhelm U. Liquid Hydrogen: Fuel of the Future. Springer-Verlag; 1992.

[20] Wolf J. Liquid hydrogen technology for vehicles. Handbook of Fuel Cells, John Wiley & Sons, Ltd; 2010.
[21] Amaseder F, Krainz G. Liquid Hydrogen Storage Systems Developed and Manufactured for the First Time for Customer Cars. Warrendale, PA: SAE International; 2006.
[22] Younglove BA. Thermophysical Properties of Fluids. 1. Argon, Ethylene, Parahydrogen, Nitrogen, Nitrogen Trifluoride, and Oxygen. American Institute of Physics; 1982.
[23] Petitpas G, Aceves SM. Hydrogen Storage in Pressure Vessels: Liquid, Cryogenic, and Compressed Gas. Hydrogen Storage Technology, Materials and Applications, Boca Raton: Taylor & Francis; 2012, p. 91.
[24] Aceves SM, Espinosa-Loza F, Ledesma-Orozco E, Ross TO, Weisberg AH, Brunner TC, et al. High-density automotive hydrogen storage with cryogenic capable pressure vessels. International Journal of Hydrogen Energy 2010;35:1219–26.
[25] Matthews MJ, Petitpas G, Aceves SM. A study of spin isomer conversion kinetics in supercritical fluid hydrogen for cryogenic fuel storage technologies. Applied Physics Letters 2011;99:081906.
[26] Stavila V, Klebanoff LE, Vajo JJ, Chen P. Development of On-Board Reversible Complex Metal Hydrides for Hydrogen Storage. Hydrogen Storage Technology, Materials and Applications, Boca Raton: Taylor & Francis; 2012, p. 133–212.
[27] Graetz J, Wolstenholme DJ, Pez GP, Klebanoff LE, Mc Grady MC, Cooper AC. Development of Off-board Reversible Hydrogen Storage Materials. Hydrogen Storage Technology, Materials and Applications, Boca Raton: Taylor & Francis; 2012, p. 239.
[28] Chao B, Klebanoff LE. Hydrogen Storage in Interstitial Metal Hydrides,". Hydrogen Storage Technology, Materials and Applications, Boca Raton: Taylor & Francis; 2012, p. 109.
[29] Ahluwalia RK, Peng JK. Automotive hydrogen storage system using cryo-adsorption on activated carbon. International Journal of Hydrogen Energy 2009;34:5476–87.
[30] Richard M-A, Cossement D, Chandonia P-A, Chahine R, Mori D, Hirose K. Preliminary evaluation of the performance of an adsorption-based hydrogen storage system. AIChE Journal 2009;55:2985–96.
[31] Richard M-A, Bénard P, Chahine R. Gas adsorption process in activated carbon over a wide temperature range above the critical point. Part 1: modified Dubinin-Astakhov model. Adsorption 2009;15:43–51.
[32] Ardelean O, Blanita G, Borodi G, Lazar MD, Misan I, Coldea I, et al. Volumetric hydrogen adsorption capacity of densified MIL-101 monoliths. International Journal of Hydrogen Energy 2013;38:7046–55.
[33] Tamburello D, Motyka T, Chahine R, Hardy B, Kesterson M, Corgnale C. SRNL Technical Work Scope for the Hydrogen Storage Engineering Center of Excellence, Design and Testing of Adsorbent Storage Systems 2013.
[34] Sudik A, Veenstra M, Yang J. Ford/BASF-SE/UM Activities in Support of the Hydrogen Storage Engineering Center of Excellence 2011.
[35] Chahine R, Bénard P, Dundar E, Ubaid S, Xiao J. Hydrogen Adsorption Storage Systems : From Molecular Design to System Design 2012.
[36] Purewal J, Liu D, Sudik A, Veenstra M, Yang J, Maurer S, et al. Improved Hydrogen Storage and Thermal Conductivity in High-Density MOF-5 Composites. J Phys Chem C 2012;116:20199–212.
[37] Streppel B, Hirscher M. BET specific surface area and pore structure of MOFs determined by hydrogen adsorption at 20 K. Phys Chem Chem Phys 2011;13:3220–2.
[38] Kumar S, Raju M, Senthil Kumar V. System simulation models for on-board hydrogen storage systems. International Journal of Hydrogen Energy 2012;37:2862–73.
[39] Chakraborty A, Kumar S. Thermal management and desorption modeling of a cryo-adsorbent hydrogen storage system. International Journal of Hydrogen Energy 2013;38:3973–86.
[40] Hardy B, Corgnale C, Chahine R, Richard M-A, Garrison S, Tamburello D, et al. Modeling of adsorbent based hydrogen storage systems. International Journal of Hydrogen Energy 2012;37:5691–705.

[41] Aceves SM. III.14 Thermodynamic Modeling of Rapid Low Loss Cryogenic Hydrogen Refueling. DOE Hydrogen and Fuell Cells Programm FY 2011 Annual Progress Report, Oak Ridge, TN: U.S. Department of Energy; 2011, p. 358.
[42] Son D-S, Chang S-H. Evaluation of modeling techniques for a type III hydrogen pressure vessel (70 MPa) made of an aluminum liner and a thick carbon/epoxy composite for fuel cell vehicles. International Journal of Hydrogen Energy 2012;37:2353–69.
[43] Roylance D. Netting analysis for filament-wound pressure vessels 1976.
[44] Swanson SR, editor. Introduction to design and analysis with advanced composite materials. Upper Saddle River, N.J.: Prentice Hall; 1997.
[45] Barbero EJ. Introduction to Composite Materials Design, Second Edition. CRC Press; 2010.
[46] Simmons K. Enhanced Materials and Design Parameters for Reducing the Cost of Hydrogen Storage Tanks 2013.
[47] Paggiaro R, Michl F, Bénard P, Polifke W. Cryo-adsorptive hydrogen storage on activated carbon. II: Investigation of the thermal effects during filling at cryogenic temperatures. International Journal of Hydrogen Energy 2010;35:648–59.
[48] Mintz M, Elgowainy A, Gillette J. H2A Delivery Scenario Analysis Model Version 2.0* (HDSAM 2.0) User's Manual. Argonne National Laboratory, Center for Transportation Research, prepared for U.S. Department of Energy, Office of Hydrogen, Fuel Cells and Infrastructure Technologies, http://www.hydrogen.energy.gov/h2a_delivery.html n.d.